MODELING THE EFFECT OF SULFUR LOADING ON THE ELECTROCHEMICAL PERFORMANCE OF A LITHIUM-SULFUR BATTERY

by

Oğuztan Uzun

B.S., Chemical Engineering, Boğaziçi University, 2018

Submitted to the Institute for Graduate Studies in
Science and Engineering in partial fulfillment of
the requirements for the degree of
Master of Science

Graduate Program in Chemical Engineering

Boğaziçi University

2023

ACKNOWLEDGEMENTS

I am incredibly grateful to my supervisor, Assoc. Prof. Dr. Damla Eroğlu Pala, for her patience, help, guidance, and kindness. I am also thankful to my partner Seçkin Çelik for her encouragement and love and also to my friends, Onat Yılmaz, Duygu Demir, and Arda Fırat Demirpençe, for their valuable insights and support. I would be remiss in not mentioning my parents, Necla and Kamil Uzun, my sister Duygu Uzun Tuzcu, my brother-in-law Efe Tuzcu and our new family member Tayga Tuzcu. Last but not least, I want to thank Büşra Abdulkadiroğlu for her support during my study.

ABSTRACT

MODELING THE EFFECT OF SULFUR LOADING ON THE ELECTROCHEMICAL PERFORMANCE OF A LITHIUM-SULFUR BATTERY

Lithium-sulfur (Li-S) batteries are a promising solution for the efficient energy storage demand due to their high theoretical specific energy. Also, Li-S battery has inexpensive raw materials that are naturally abundant and non-toxic. For these advantages, they are considered an alternative to Li-ion batteries. However, they also have disadvantages, such as low cycle life and considerable self-discharge. The complex electrochemical reactions in Li-S batteries need to be better understood and defining the significant parameters and their effects are required to overcome these challenges. So different studies are focusing on finding the optimum cathode design parameters. This study investigates the effect of one of the critical cathode design parameters, sulfur loading, on the electrochemical performance of a Li-S battery. Although sulfur is an electrochemically active material in the cell, it negatively affects cell performance at high loadings since it is insoluble and insulating. In order to increase the conductivity and surface area, carbon is typically used in the cathode. However, an inert material like carbon can lower the energy density. So, the optimum cathode design for high S utilization and high energy density is still under investigation because of the Li-S battery's complex mechanisms. For estimating the effect of S loading, computational algorithms were used in this study; simplified zero-dimensional and more complex one-dimensional electrochemical models were selected, and the models' response in predicting the impact of S loading on the discharge performance was compared. The zero-dimensional model could not capture the effect of S loading on the discharge capacity; however, the one-dimensional model successfully predicted the experimental trends. Furthermore, a sensitivity analysis was done on both models for different model parameters to discuss the reasons for the differences between the models.

ÖZET

LİTYUM-KÜKÜRT PİLİNİN ELEKTROKİMYASAL PERFORMANSI ÜZERİNDE KÜKÜRT YÜKLEMENİN ETKİSİNİN MODELLENMESİ

Lityum-kükürt (Li-S) piller, yüksek teorik özgül enerjileri nedeniyle verimli bir enerji depolama sistemi olarak umut vermektedir. Ek olarak, Li-S piller, doğal olarak bol ve toksik olmayan ucuz hammaddelere sahiptir. Bu avantajlar nedeniyle Li-iyon pillere bir alternatif olarak kabul edilirler. Bununla birlikte, düşük çevrim ömrü ve kendi kendine deşarj gibi dezavantajları da vardır. Li-S pillerdeki elektrokimyasal reaksiyonların açıklığa kavuşturulması ve önemli parametrelerin ve bunların etkilerinin tanımlanması gerekmektedir. Bu nedenle, katot tasarımında optimum parametreleri bulmak için odaklanan farklı çalışmalar vardır. Bu çalışma, kritik bir katot tasarım parametresi olan kükürt yükleme miktarının Li-S pilinin elektrokimyasal performansına etkisini araştırmaktadır. Kükürt hücrede elektrokimyasal olarak aktif bir madde olmasına rağmen, çözünmez ve yalıtkan olduğundan yüksek konsantrasyonlarda hücre performansını olumsuz etkiler. İletkenliği ve yüzey alanını artırmak için katotta karbon kullanılır. Bununla birlikte, karbon gibi inert malzemeler enerji yoğunluğunu azaltabilir. Dolayısıyla, Li-S pilindeki karmaşık mekanizmalar nedeniyle hem yüksek kapasite hem de enerji yoğunluğu için gereken optimum katot tasarım parametreleri hala araştırılmaktadır. S yükleme miktarının etkilerini tahmin etmek için bu çalışmada hesaplamalı algoritmalar kullanılmıştır; basitleştirilmiş sıfır boyutlu ve daha karmaşık tek boyutlu elektrokimyasal modeller seçilmiş ve bu modellerin S yükleme miktarının deşarj performansına etkisi üzerine tahminleri karşılaştırılmıştır. Sıfır boyutlu model S yükleme miktarının deşarj kapasitesi üzerine etkisini yakalayamazken, tek boyutlu model, deneysel eğilimleri başarıyla tahmin etmiştir. Ayrıca her iki modelde de farklı parametreler için duyarlılık analizi yapılarak modeller arasındaki farklar tartışılmıştır.

TABLE OF CONTENTS

LIST OF FIGURES

LIST OF TABLES

LIST OF SYMBOLS

a	Electrochemically active area in the cathode, $m^2\ m^{-3}$
a_0	Initial specific surface area of the cathode, $m^2\ m^{-3}$
a_r	Active reaction area per cell, m^2
b	Bruggeman's coefficient
B	Binder
C	Carbon
C_i	Concentration of species *i*, mol m^{-3}
$C_{i,ref}$	Reference concentration of species , mol m^{-3}
D_i	Diffusion coefficient of species *i*, $m^2\ s^{-1}$
e	Liquid-Phase
E_{cell}	Cell voltage, V
E_H, E_L	Equilibrium potentials, V
E_H^0, E_L^0	Standard potentials, V
F	Faraday constant, C mol^{-1}
f_H	Dimensionality factor *H*, g L mol^{-1}
f_L	Dimensionality factor *L*, g L mol^{-1}
H	High Voltage Plateau
i	Species In The System
I	Current density, A cm^{-2}
I_{app}	Applied current density, A m^{-2}
$i_{0,jref}$	Exchange current density of electrochemical reaction *j*, A m^{-2}
i_e	Liquid-phase current density, A m^{-2}
$i_H\ i_L$	Current contributions, A
$i_{H,0}\ i_{L,0}$	Exchange current density, A m^{-2}
i_j	Current density due to electrochemical reaction *j*, A m^{-2}
i_s	Solid-phase current density, A m^{-1}
j	Electrochemical Reaction in the System
k	Precipitate
k_k	Precipitation rate constant of *k*, units vary
k_p	Precipitation rate, s^{-1}

k_s	Shuttle constant, s^{-1}
$K_{sp,k}$	Solubility product of precipitate k, units vary
L	Thickness of the cathode, m / Low Voltage Plateau
m_s	Mass of active sulfur per cell, g
M_{S_8}	Molar mass S_8, g mol^{-1}
n_e	Electron number per reaction, -
n_i	Number of *S* atoms in polysulfide *i*, -
N_i	Flux of species *i*, mol m^{-2} s^{-1}
n_j	Number of electrons transferred in electrochemical reaction *j*, -
$p_{i,j}$	Anodic reaction order of species *i* in electrochemical reaction *j*, -
R	Gas constant, J mol^{-1} K^{-1}
R_i	Production/consumption rate of species *i*, mol m^{-3} s^{-1}
r_i	Production/consumption rate of species *i* due to electrochemical reactions, mol m^{-3} s^{-1}
R'_k	Production rate of precipitate *k*, mol m^{-3} s^{-1}
s	Solid-Phase
S_*^{2-}	S^{2-} saturation mass, g
$s_{i,j}$	Stoichiometric coefficient of species *i* due to electrochemical reaction *j*, -
S_p	Mass of precipitated S^{2-}, g
T	Temperature, K
t	Time, s
U_j^0	Standard open-circuit potential of electrochemical reaction *j*, V
$U_{j,ref}$	Open-circuit potential of electrochemical reaction *j*, V
V	Cell voltage, V
v	Electrolyte volume per cell, L
$\tilde{V}_k$	Molar volume of precipitate *k*, m^3 mol^{-1}
x	Distance from the separator through the cathode, μm
z_i	Charge number of species *i*, -
α_{a_j}	Anodic transfer coefficient of reaction j

α_{c_j}	Cathodic transfer coefficient of reaction j
$\gamma_{i,k}$	Number of ionic species *i* in precipitate *k*
ε	Porosity of cathode (or the electrolyte volume fraction in the cathode)
ε_B	Volume fraction of binder in the cathode
ε_C	Volume fraction of carbon in the cathode
$\varepsilon_{initial}$	Initial cathode porosity
ε_k	Volume fraction of precipates in the cathode
ε_{Li_2S}	Volume fraction of precipitate $Li2S(s)$ in the cathode
ε_{ref}	Reference porosity of cathode
$\varepsilon_{S_{8(s)}}$	Volume fraction of $S8(s)$ in the cathode
η_H	Overpotential for high voltage plateau
η_L	Overpotential for low voltage plateau
ρ_B	Density of binder in cathode, g/cm3
ρ_C	Density of carbon in cathode, g/cm3
$\rho_{cathode}$	Density of cathode, g/cm3
$\rho_{Electryolte}$	Density of electrolyte in cathode, g/cm3
ρ_s	Density of sulfur in cathode, g/cm3
σ	Effective electronic conductivity of cathode, S/m
ϕ_e	Potential of liquid phase, V
ϕ_s	Potential of solid phase, V
ω_B	Weight fraction of binder in the cathode
ω_C	Weight fraction of carbon in the cathode
ω_S	Weight fraction of sulfur in the cathode
$*$	Saturation
0	Initial

LIST OF ACCRONYMS/ABBREVIATIONS

app	Applied
C/S	Carbon to sulfur ratio
$cathode$	Cathode Electrode
$cell$	Battery Cell
E/S	Electrolyte volume to sulfur ratio
FORTRAN	Formula Translating System
OCP	Open circuit potential
ref	Reference
sp	Solubility Product

1. INTRODUCTION

In the next era of mobility, the demand for energy storage is increasing worldwide. Lithium-sulfur (Li-S) batteries seem to be a promising solution with their theoretical specific energy of 2567 Wh kg-1 [1]. The advantage of the Li-S battery is not limited to its theoretical energy; the raw materials are inexpensive, naturally abundant, and non-toxic. For those reasons, they are considered an alternative to Li-ion batteries. Li-S cells generally are made of the Li metal anode, a porous separator, and the porous Sulfur-Carbon cathode filled with an organic electrolyte. The reactions in the Li-S cell are complicated since the reduction of solid sulfur has multi-steps, and polysulfide interactions are not clearly understood. However, the net electrochemical reaction is known as shared in Equation (1.1). Although six electrochemical and five precipitation/dissolution reactions are proposed in the literature, the effect of the reactions on cell performance is controversial. The mentioned reaction mechanism can be found as below;

$$16Li + S_8 \rightarrow 8Li_2S \quad (1.1)$$

$$Li \leftrightarrow Li^+ + e^- \quad (1.2)$$

$$\frac{1}{2}S_{8(l)} + e^- \leftrightarrow \frac{1}{2}S_8^{2-} \quad (1.3)$$

$$\frac{3}{2}S_8^{2-} + e^- \leftrightarrow 2S_6^{2-} \quad (1.4)$$

$$S_6^{2-} + e^- \leftrightarrow \frac{3}{2}S_4^{2-} \quad (1.5)$$

$$\frac{1}{2}S_4^{2-} + e^- \leftrightarrow S_2^{2-} \quad (1.6)$$

$$\frac{1}{2}S_2^{2-} + e^- \leftrightarrow S^{2-} \quad (1.7)$$

$$S_{8(l)} \leftrightarrow S_{8(s)} \quad (1.8)$$

$$2Li^+ + S_8^{2-} \leftrightarrow Li_2S_{8(s)} \quad (1.9)$$

$$2Li^+ + S_4^{2-} \leftrightarrow Li_2S_{4(s)} \quad (1.10)$$

$$2Li^+ + S_2^{2-} \leftrightarrow Li_2S_{2(s)} \quad (1.11)$$

$$2Li^+ + S^{2-} \leftrightarrow Li_2S_{(s)}. \quad (1.12)$$

An illustration of the described Li-S cell can be seen in Figure 1.1. Li metal is the anode in the cell, and during discharge, the anode is oxidized, as expressed in Equation (1.2). The cathode is a sulfur-based electrode, and the produced free electrons move from the anode side to the cathode side through an external circuit. When the free electrons reach the cathode, the solid sulfur is reduced as Equations (1.3)-(1.8). At the same time, the oxidized

ions migrate to the cathode side through the porous separator. By the mentioned mechanism, highly soluble high-order polysulfides are formed. Still, insoluble and insulating low-order polysulfides are also formed at the end of the discharge. Since these polysulfides can negatively impact cell performance, the mechanisms of forming these intermediate products are critical.

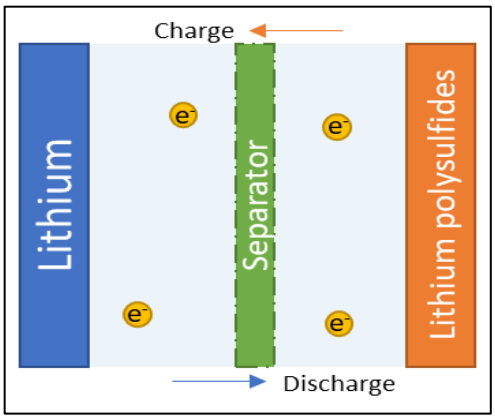

Figure 1.1. Schematic diagram of Li/S cell electrochemistry.

A typical discharge curve for a Li-S battery has two voltage plateaus; the first is higher than the other. The reactions shown in Equations (1.3)-(1.4) and (1.5)-(1.7) [2] are responsible for the high and low voltage plateaus, respectively. Lithium polysulfide formation starts in the high voltage plateau, and the effect can be seen by the voltage drop between the plateaus. The voltage drop can be caused by increasing viscosity in the electrolyte due to lithium polysulfide concentration [3]. The formation of insoluble and insulating low-order polysulfides causes a sharp voltage drop at the end of the discharge[4].

Even with the advantages mentioned above of a Li-S cell, some difficulties are ahead on the way to mass commercialization. The problems at the moment are fast capacity fading and poor cycle life. Sulfur itself and low-order polysulfide products are insulators and decrease the conductivity of the electrolyte. In addition, the insoluble precipitates form at the cathode surface during discharge, and the active surface of the cathode is reduced over time [5]. Moreover, the soluble polysulfides, intermediate products, can diffuse through the separator layer and reach the anode. If that happens, the soluble polysulfides can react with the Li metal and diffuse back to their initial location. In the literature, the mentioned

mechanism is called the shuttle phenomenon, which causes passivation of the active cathode surface, self-discharge of the cell, and a reduction in the cycle performance.

Furthermore, the surface area of the Li anode can increase with each cycle, and the contact area between the electrolyte and anode can be increased. Since the Li metal has high reactivity, this will enhance the reaction between Li and the electrolyte. As a consequence, the reaction will consume Li metal or electrolyte. Therefore, studies are focused on specialized materials for Li-S cells to prevent the mentioned difficulties.

The Li-S cell design parameters are crucial because of this complex reaction mechanism. The studies show that the cathode design parameters have optimum values for expected good performance; otherwise, Li-S cells can show dramatically low performance [4,5]. The cathode design parameters can impact the battery performance at the material, cell, and system levels. The sulfur loading, the carbon-to-sulfur ratio (C/S), and the electrolyte-to-sulfur ratio (E/S) are good examples of these crucial parameters. Adding carbon increases the electronic conductivity and the surface area in the cathode, so carbon is a common ingredient in the sulfur cathode design to enhance the reaction kinetics. Hence, higher C/S ratios until a threshold show better sulfur utilization, cell capacity, and cycle life performance. After this threshold, the excess amount of carbon decreases the cell's energy density because carbon is not an active material in cell reactions. The E/S ratio also affects the cycle life, capacity, and energy density. The reaction kinetics and shuttle phenomena can be controlled by electrolyte level. The reaction kinetics and discharge capacity are affected positively in excess electrolyte amounts, while energy density and cycle life are affected negatively. Lastly, sulfur loading is vital in cell performance since it is the active material while acting as an insulator. The study from Eroglu et al. shows that high sulfur loadings are necessary to reach efficient battery design regarding cost and energy [6]. So, each cell design parameter has a “trade-off” between high capacity and cycle life with high energy density. Consequently, their impact on the reaction mechanisms and, thus, on the performance of the Li-S battery should be investigated thoroughly.

1.1. Scope of the Current Work

Due to the highly complex reaction and polysulfide shuttle mechanisms in the cathode, the performance of a Li-S battery at the material, cell, and system level depends significantly on the cell design. As described above, one of the critical cell design parameters is S loading, which can affect the discharge capacity, cycle life, energy density, and specific energy of the Li-S battery. As will be discussed in the following section, there are various models to predict the Li-S battery performance. Since multi-component Li-S chemistry is very complex, sometimes the critical parameters are simplified, and sometimes the mathematical models are modified to match the experimental data. However, a limited number of studies are trying to understand whether the models can capture the impact of cell design, specifically the sulfur loading, on the Li-S battery performance.

This study investigates the effect of S loading on the reaction kinetics and electrochemical performance. For that purpose, a simplified zero-dimensional and a more complex one-dimensional electrochemical model are selected, and the models' response in predicting the impact of S loading on the discharge performance is compared. Even though zero-dimensional models have the advantage of fewer assumed parameters, they may not capture some effects due to neglecting specific mechanisms in the cell. On the other hand, one-dimensional models are more complex and can include the necessary mechanisms in the cell. However, because of this high level of complexity, there are many assumed model parameters and thus the need for curve-fitting. Herein, a zero-dimensional model by Marinescu et al. [7] and, a one-dimensional model by Abdulkadiroglu, Bektas, and Eroglu[8], a modified version of the model by Erisen and Eroglu [9], were selected. The models have similarities in the number of precipitated materials and electrochemical reactions. We investigated whether the models can predict the cell behavior with different S loadings and if the experimental trends on the dependence of discharge performance on the S loading are captured in the model predictions. In addition, a detailed sensitivity analysis was done on the selected models to understand the model's response for each parameter variation.

The cathode design parameters are typically not independent, and therefore, the S loading in the cathode can be varied in different ways. The first way is to keep the cathode

thickness fixed while varying the carbon and sulfur weight percentages in the cathode (so the C/S ratio changes). The second way is to increase the cathode thickness with increasing sulfur loading so that the C/S ratio remains constant. In this work, both scenarios were investigated. The C/S and E/S ratios were kept constant while examining the influence of S loading.

2. LITERATURE REVIEW

2.1. Previous Studies on Electrochemical Models of the Li-S Battery

The mathematical models of the Li-S battery can be very complex. Current one-dimensional mathematical models are commonly based on the previous model derived by Kumaresan et al. [1]. The model consists of a detailed mechanism including six electrochemical and five precipitation/dissolution reactions, which are given in Equations (1.2)-(1.12). In this multi-component system, the mass flux of the species is obtained by diffusion and migration. The model is one-dimensional, and the variation of the concentrations of the species concerning position and time is taken into account. The mass balance equations include the production and consumption rates due to the electrochemical and precipitation/dissolution reactions. The model predicts the voltage profile of a Li-S battery at a constant-current discharge. The change in the specific area of the cathode surface due to a change in porosity is also considered. The reaction kinetics are calculated by the Butler-Volmer equation. Due to precipitation/dissolution reactions, the components' production rate is involved in the conservation of species equations using the solubility rate constants. All in all, the presented model provides a variety of information about the concentration of species, porosity of the electrode, and volume fractions of precipitates as a function of time and space, and it predicts the discharge profile of a Li-S cell. Projected discharge profiles show high and low-voltage plateaus; the species that dominate these plateaus are predicted in the study. However, the aforementioned shuttle phenomenon is ignored in the presented model.

In the literature, sensitivity analyses are performed on the abovementioned mathematical model. One study focuses on the effects of discharge current and cathode conductivity on the Li-S discharge behavior [10]. The analysis found that electrochemical reactions occur in an order, which means one reaction starts after the previous one is completed. Also, a significant capacity loss is seen at low discharge rates due to the slow dissolution of elemental sulfur; the minimum conductivity required to operate the cell is determined. The authors observe a difference between the model predictions and the experimental data regarding the discharge profile, particularly at the second plateau, and

they suggest that this is due to the model ignoring the passivated active surface. In another analysis, the effects of precipitation reaction kinetics and sulfur content are investigated [11]. After observing the effect of rate constants, “critical intervals” for each rate constant are determined. Beyond these intervals, the cell performance shows nonlinear behavior. The paper suggests a modification for the precipitation equations. The same group performs another sensitivity analysis on the electrochemical reaction kinetics, transport properties, and charging issues [12]. The paper suggests that the reduction of elemental sulfur and S_2^{2-} shows the most significant effects on cell performance. When diffusion coefficients are assumed to be lower than usual, there is non-uniformity regarding the active and precipitated material during discharge. Last but not least, these analyses show that the model cannot predict the charging profile of a Li-S cell due to the low solubility of $Li_2S_{(s)}$.

A zero-dimensional model is derived for Li-S batteries to investigate the charge and discharge profiles by Marinescu et al. [7]. The model includes a different reaction mechanism than the previous one. There are two electrochemical reactions involved in the model, as given below. This reaction mechanism is previously proposed by Mikhaylik and Akridge for understanding and predicting the effect of the shuttle phenomenon [13]:

$$S_8^0 + 4e^- \leftrightarrow 2S_4^{2-} \quad (2.1)$$

$$S_4^{2-} + 4e^- \leftrightarrow 2S^{2-} + S_2^{2-}. \quad (2.2)$$

In these models, the reaction mechanism is simplified into two electrochemical reactions; a single reaction for each of the two discharge plateaus is proposed. By doing this, using hard-to-obtain physical and chemical parameters can be minimized while developing the model. Butler-Volmer equations and dissolution/precipitation constants define the reaction kinetics. Moreover, the shuttle phenomenon is included in the model by a shuttle constant. The discharge and charge profiles of the Li-S battery can be successfully projected with the proposed model. The paper also finds that dissolution can be the limiting step in the process when the charging current is high.

Yoo et al. propose a modification to the model developed by Kumaresan et al. for investigating the cycling performance of a Li-S cell [14]. The presented model is compared with the experimental studies; the reactions considered in the paper are mentioned in Equations (1.1)-(1.8), (1.10)-(1.11). The reduction reactions of higher polysulfides are

examined to observe the effect of the shuttle phenomenon, and the precipitation/dissolution reaction kinetics is based on a previous model [1] and modified for numerical stability. $Li_2S(s)$ and $S_{8(s)}$ are the most critical solid species for predicting electrochemical performance compared to experimental data. The high rate constant of polysulfide reduction reactions leads to an overcharging problem, and the increased polysulfide solubility does not allow a complete charge.

Another work studies the partial cycling of the Li-S battery by combining experimental and theoretical methods to find the relationship between the sulfur loss, capacity fade, and shuttle phenomenon [15]. The presented model is also based on Equations (2.1)-(2.2). The proposed model is beneficial for investigating reversible and irreversible capacity loss during charging. The paper shows that low charging rates result in an irreversible capacity loss due to the polysulfide shuttle. On the other hand, high rates result in a reversible loss since an accumulation in the precipitated species is observed, and they can be re-dissolved by charge.

Zhang et al. propose that the electrolyte resistance is dependent on the concentrations of species [16] and derive a model for observing the effect of electrolyte resistance and precipitation kinetics on the voltage profile. However, the model does not consider the mass transport and charge-localization effects, such as the shuttle phenomenon. The reactions used in the model are shown in Equations (1.2)-(1.7) and (1.12). The presented model shows how the electrolyte is affected by the concentrations due to precipitation. The precipitated components reduce the electrochemically active area. So, it is suggested to consider the relationship between polysulfide concentration and conductivity.

A recent study investigates the limiting factors on the discharge rate capability of a Li-S cell [17]. The results show that mass transport limits the rate capability during discharge rather than charge transport, which was assumed as the limiting factor in the previous studies. Also, a simple model is presented with the expressions of $Li_2S_{(s)}$ surface coverage.

Another study by Andrei et al. develops a rate-dependent nucleation theory for Li-S cells [18]. Although the analysis follows the Kolmogorov-Avrami approach for nucleation, the related equations are expressed as differential equations. The mathematical model

consists of Equations (1.2)-(1.7) for the electrochemical reactions and Equations (1.8)-(1.12) for the dissolution/precipitation reactions, in addition to the reaction which can be found below,

$$2Li^+ + S_6^{2-} \leftrightarrow Li_2S_{6(s)}. \quad (2.3)$$

In the model, each nucleation seed at its specific location is defined, and then the change in the surface coverage is estimated. As mentioned before, nucleation is rate-dependent; higher discharge rates result in higher nucleation rates. However, at low discharge rates, the number of nucleation particles is fewer, but the particles can be larger than in the high discharge examples.

A one-dimensional concentration-dependent model is presented in a recent study by Erisen and Eroglu [9]. Although the reaction mechanism is simplified compared to the ones mentioned above, the most significant species that affect the performance of Li-S cells are involved in the reaction mechanism. The electrochemical and dissolution/precipitation reactions can be found below:

$$S_{8(s)} \leftrightarrow S_8^0 \quad (2.4)$$

$$\frac{1}{4}S_8^0 + e^- \leftrightarrow \frac{1}{2}S_4^{2-} \quad (2.5)$$

$$\frac{1}{6}S_4^{2-} + e^- \leftrightarrow \frac{2}{3}S^{2-} \quad (2.6)$$

$$2Li^+ + S^{2-} \leftrightarrow Li_2S_{(s)}. \quad (2.7)$$

2.2. Previous Studies on the S Loading Effect on Li-S Battery Performance

There are different studies about cell design parameters in the literature with different perspectives. Herein, the summary will be shared.

The study by Erisen and Eroglu [9] examines vital design parameters regarding their effects on the Li-S cell performance. The parameters mentioned earlier are the electrolyte-to-sulfur (E/S) and carbon-to-sulfur (C/S) ratios. Although the results show that the battery performance is enhanced with increasing C/S and E/S ratios, the effect of these parameters is not very significant at higher levels. A recent study by Abdulkadiroglu, Bektas, and Eroglu proposed a novel definition of the active cathode area. With this modification, the definition

can include the cell's carbon amount and reference porosity. The model can better predict the effect due to cell design parameters such as the E/S, the C/S ratios, and S loading.

Another study by Michaelis et al. [19] shows the experimental results and model predictions on varying C/S ratios in the cell. Lower C/S ratios lead to low discharge capacity, and the study reports higher sulfur accumulation on the cathode surface at high S loadings.

Another study by Bilal and Eroglu [18] investigates the impact of C/S and E/S ratios on a Li-S cell's discharge, cycling, and pack-level performance. The study reports that the C/S ratio significantly affects cycling performance. The paper also suggests the optimum ratios using model predictions for cell and system levels.

Also, some studies focus on S loading experimentally. Kang et al. [20] suggest an optimum E/S ratio and S loading level for good cycling and energy density. The study from Sun et al. [21] suggests a maximum threshold for S loading for better performance on discharge capacity and investigates the reason behind the capacity reduction at higher sulfur contents in the cathode. The study from Ding et al. [22] investigates the Li-S cells' cycling and discharge capacity performances. The study varies the S loading at the same C/S ratio, and the paper suggests using specialized materials to reach higher performances at high S loadings.

3. MODEL DEVELOPMENT

In this section, the electrochemical battery models used in this study to estimate the Li-S battery performance are shared in detail. In the rest of the part, detailed equations can be found for a concentration-independent zero-dimensional and a concentration-dependent one-dimensional electrochemical model.

FORTRAN programming language is used for running the simulations. Model predictions and sensitivity analysis are used to compare the models' effectiveness in capturing the critical parameters' effect, especially sulfur loading, on the discharge behavior of a Li-S battery.

During this study, the algorithm from Newman and Thomas-Alyea's [23] study is used in FORTRAN. The algorithm uses Taylor’s series for estimating time and space-dependent functions. The equations should be linearized to be used in FORTRAN. The linearization procedure is shared at the end of the part.

3.1. Zero-Dimensional Electrochemical Model for a Li-S Cell

The provided model by Marinescu et al. [8] is selected for this study as a simple electrochemical model. The time interval for the simulation is selected as 0.1 seconds, and the simulation uses 103 node points. This model contains two electrochemical reactions, dissolution-precipitation kinetics and shuttle phenomenon, with five different species. The assumptions of the model are listed below.

- Single electrochemical reaction for each discharge region (high and low voltage plateaus).
- Solid sulfur is fully dissolved.
- Li anode overpotential is considered small, and it is neglected.
- Shuttle and precipitation reactions occur during discharge.
- Shuttle and precipitation kinetics are defined by rate constants.

- During discharge, the discharge current is assumed constant.
- Cathode reactions occur at the same time and are symmetric. So, the transfer coefficients are assumed to be 0.5.
- No double-layer effects.

The discharge reactions take place under a two-step chain mechanism as follows:

$$S_8^0 + 4e^- \leftrightarrow 2S_4^{2-} \tag{3.1}$$
$$S_4^{2-} + 4e^- \leftrightarrow 2S^{2-} \downarrow + S_2^{2-}. \tag{3.2}$$

Equation (3.1) dominates the high-voltage plateau, and Equation (3.2) dominates the low-voltage plateau. For the equilibrium potentials, Nernst equations are used like below:

$$E_H = E_H^0 + \frac{RT}{4F} \ln\left(f_H \frac{S_8^0}{(S_4^{2-})^2}\right) \tag{3.3}$$
$$E_L = E_L^0 + \frac{RT}{4F} \ln\left(f_L \frac{S_4^{2-}}{(S^{2-})^2 S_2^{2-}}\right) \tag{3.4}$$

where E_H^0 and E_L^0 are standard potentials for the two-step chain reactions, respectively, R is the gas constant, T is temperature, and F is the Faraday constant. f_L and f_H are constants derived during the model development [7] that are used to calculate the sulfur mass instead of concentrations. The constants mentioned above are expressed as

$$f_H = \frac{n_{S_4}^2 M_{S_8} v}{n_{S_8}} \tag{3.5}$$
$$f_L = \frac{n_S^2 n_{S_2} M_{S_8}^2 v}{n_{S_4}}. \tag{3.6}$$

In these expressions, M_{S_8} is the molar mass of sulfur, v is the electrolyte volume, and n numbers are the number of atoms for the molecules or ions mentioned in the subscript.

For the reaction kinetics, the Butler-Volmer equations are used. The kinetics of high and low-voltage plateau reactions are expressed as follows:

$$i_H = 2i_{H,0} a_r \sinh \frac{n_e F \eta_H}{2RT} \tag{3.7}$$
$$i_L = 2i_{L,0} a_r \sinh \frac{n_e F \eta_L}{2RT}, \tag{3.8}$$

where $i_{H,0}$ and $i_{L,0}$ are exchange current densities, a_r is the active surface area for each reaction, n_e represents the number of electrons transferred, and η_L, η_H are the surface overpotentials.

The driving force for the reactions is the potential difference between the Nernst potential and the surface overpotential. Hence, they are used for estimating cell performance. The equations for the high and low-voltage plateaus can be written as

$$\eta_H = V_{cell} - E_H \tag{3.9}$$
$$\eta_L = V_{cell} - E_L. \tag{3.10}$$

By using the conservation of charges, the reaction current densities will be equal to the applied current as follows:

$$I = i_H + i_L. \tag{3.11}$$

The applied current is defined below to capture the effect of sulfur loading,

$$I = m_S \times C\text{-}rate, \tag{3.12}$$

where m_s is active sulfur mass per cell and *C-rate* represents the desired charge rate depending on the sulfur mass. For example, 1C is used as 1675 mA per gram of sulfur for full discharge in 1 hour.

Last but not least, the change in the concentration of species involved in the two-step reaction mechanism with time is calculated as follows:

$$\frac{dS_8^0}{dt} = -\frac{n_{S_8} M_{S_8}}{n_e F} i_H - k_s S_8^0 \tag{3.13}$$
$$\frac{dS_4^{2-}}{dt} = \frac{n_{S_8} M_{S_8}}{n_e F} i_H + k_s S_8^0 - \frac{n_{S_4} M_{S_8}}{n_e F} i_L \tag{3.14}$$
$$\frac{dS_2^{2-}}{dt} = \frac{n_{S_2} M_{S_8}}{n_e F} i_L \tag{3.15}$$
$$\frac{dS^{2-}}{dt} = \frac{2 n_S M_{S_8}}{n_e F} i_L - \frac{1}{v \rho_S} k_p S_p (S^{2-} - S_*^{2-}) \tag{3.16}$$
$$\frac{dS_p}{dt} = \frac{1}{v \rho_S} k_p S_p (S^{2-} - S_*^{2-}). \tag{3.17}$$

In these expressions, the shuttle and precipitation effects are also considered through the shuttle and precipitation rate constants k_s and k_p, respectively. Hence, S_p is the precipitated sulfur mass, ρ_S is the density of precipitated sulfur, and S_*^{2-} is the saturation threshold.

3.1.1. Initial Conditions

The initial conditions used in the model by Marinescu et al. [7] can be found below for each variable.

$$S_8^0 = 0.99 m_s \tag{3.18}$$

$$S_4^{2-} = \left(\frac{f_H}{exp\left(\frac{(E_H - E_H^0)4F}{RT} \right)} \right)^{0.5} \tag{3.19}$$

$$S_2^{2-} = S_p + S^{2-} \tag{3.20}$$

$$S^{2-} = \left(\frac{f_L S_4^{2-}}{exp\left(\frac{(E_L - E_L^0)4F}{RT} \right)(S_2^{2-})} \right)^{0.5} \tag{3.21}$$

$$S_p = 10^{-6} m_s \tag{3.22}$$

$$E_H = V_{cell} - \eta_H \tag{3.23}$$

$$E_L = V_{cell} - \eta_L \tag{3.24}$$

$$i_H = I \tag{3.25}$$

$$i_L = 0 \tag{3.26}$$

$$V_{cell} = 2.4 \text{ V} \tag{3.27}$$

$$\eta_H = \frac{2RT}{n_e F} \operatorname{arcsin\,h}\left(\frac{-i_H}{2 i_{H,0} a_r} \right) \tag{3.28}$$

$$\eta_L = 0. \tag{3.29}$$

For Equation (3.20)-(3.21), the initial S^{2-} is unknown. Therefore mentioned equations are iterated with an estimation until the error becomes below 10^{-9}.

3.1.2. Parameters in the Model

The cell parameters in the model can be found in Table 3.1, taken from Marinescu et al. [7].

Table 3.1. Cell parameters in the zero-dimensional model.

Notation	Name	Units	Value
F	Faraday's constant	C mol^{-1}	$9.649x10^4$
M_{S_8}	Molar mass of S_8^0	g mol^{-1}	32
N_A	Avogadro number	mol^{-1}	$6.0221x10^{23}$
$n_{S_8}, n_{S_4}, n_{S_2}, n_S$	Number of S atoms in polysulfide species	-	8, 4, 2, 1
R	Gas Constant	J K^{-1} mol^{-1}	8.3145
ρ_S	Density of precipitated sulfur	g L^{-1}	$2x10^3$
a_r	Active reaction area per cell	m^2	0.960
f_H	Dimensionality factor H	g L mol^{-1}	0.7296
f_L	Dimensionality factor L	g^2 L^2 mol^{-1}	0.0665
v	Electrolyte volume per cell	L	0.0114
m_S	Mass of active sulfur per cell	g	2.7
E_H^0	Standard potential H	V	2.35
E_L^0	Standard potential L	V	2.195

Table 3.2. Cell parameters in the zero-dimensional model. (cont.)

Notation	Name	Units	Value
$i_{H,0}$	Exchange current density H	A m^{-2}	10
$i_{L,0}$	Exchange current density L	A m^{-2}	5
S_*^{2-}	Saturation mass of S2-	g	0.0001
k_p	Precipitation rate	s^{-1}	100
k_S	Shuttle constant	s^{-1}	0.0002
I	External/Applied current	A	Variable
T	Temperature	K	298

3.2. One-Dimensional Concentration-Dependent Electrochemical Model

A more complex model, which considers the change in the concentrations of the species concerning time and position, is also studied here. This model is based on the modifications of Erisen and Eroglu [9] on the model first proposed by Kumaresan et al. [1]. Compared with Kumaresan et al.'s study [1], the considered reactions are reduced significantly to simplify the model and avoid many assumed parameters. The time interval for the simulation is selected as 0.1 seconds, and the simulation uses 501 node points. The model contains two electrochemical reactions, two dissolution/precipitation reactions, and five different species. Recently Abdulkadiroglu, Bektas, and Eroglu [8] modified the model further by changing the definition of the electrochemically active area in the cathode; therefore, new suggested area descriptions and revised parameters are used herein. The assumptions belonging to this model are listed here.

- Single electrochemical reaction for each discharge region (high and low voltage plateaus).
- The model considers the porous cathode only. The separator is not considered, and the Li anode overpotential is neglected.
- Shuttle phenomena for the polysulfides are not taken into account.
- The only precipitation product during discharge is $Li_2S_{(s)}$, and precipitation kinetics are defined by using a rate constant.
- During discharge, the discharge current is assumed constant.
- Cathode reactions occur at the same time and are symmetric. So, the transfer coefficients are assumed to be 0.5.
- No double-layer effects.
- No limitation on the Li amount in the anode.

The reactions which are included in the model are shown below:

$$S_{8_{(s)}} \leftrightarrow S_8^0 \tag{3.30}$$

$$\frac{1}{4}S_8^0 + e^- \leftrightarrow \frac{1}{2}S_4^{2-} \tag{3.31}$$

$$\frac{1}{6}S_4^{2-} + e^- \leftrightarrow \frac{2}{3}S^{2-} \tag{3.32}$$

$$2Li^+ + S^{2-} \leftrightarrow Li_2S_{(s)}. \tag{3.33}$$

Equation (3.30) represents the dissolution of solid sulfur, and, Equation (3.33) represents the precipitation of the discharge product. Equations (3.31)-

(3.32) are the electrochemical reactions considered in the model. The concentrations of species depend on time and 1-D space.

Nernst-Planck equations estimate each species' change with time and position. Hence, the material balances are built using material fluxes and production/consumption rates from the electrochemical and dissolution/precipitation reactions. The species material balance is expressed as:

$$\frac{\partial \varepsilon C_i}{\partial t} = -\nabla N_i + r_i - R_i, \tag{3.34}$$

where ε is the cathode porosity and also considered as electrolyte volume fraction, C is the concentration, t is time, N is molar flux, r is the production/consumption rate from the electrochemical reaction, and R is the production/consumption rate from dissolution/precipitation reaction while subscript *i* represents the species.

The species, represented by subscript *i*, are expressed as follows.

Table 3.3. Species in the one-dimensional model.

Species	$\boldsymbol{Li^+}$	$\boldsymbol{S_8^0}$	$\boldsymbol{S_4^{2-}}$	$\boldsymbol{S^{2-}}$	$\boldsymbol{A^-}$
$\boldsymbol{i}$	1	2	3	4	5

The mass flux expression contains Fick's law of diffusion and electromigration due to the local electric field. Therefore, it is expressed as follows:

$$N_i = -D_i \nabla C_i + z_i \frac{D_i}{RT} F C_i \nabla \phi_e, \tag{3.35}$$

where D is diffusion coefficient, C is concentration, z is charge number, T is temperature, F is Faraday's constant and ϕ_e is liquid phase potential. The charge numbers for each species are shared below.

Table 3.4. Charge number for each species.

Species	$\boldsymbol{Li^+}$	$\boldsymbol{S_8^0}$	$\boldsymbol{S_4^{2-}}$	$\boldsymbol{S^{2-}}$	$\boldsymbol{A^-}$
$\boldsymbol{z}$	1	0	-2	-2	-1

The equation is shown below for species' production/consumption rate due to an electrochemical reaction,

$$r_i = -a \sum \frac{s_{i,j} i_j}{n_j F}. \tag{3.36}$$

In the equation, a is the active surface area in the cathode, s is the stoichiometric coefficient in the reaction, i is the current density, n is the number of electrons transferred in the reaction, and subscript *j* represents the related electrochemical reaction.

The rate of dissolution/precipitation reactions is given as follows:

$$R_i = \sum_k \gamma_{i,k} R'_k = \sum_k \gamma_{i,k} \left(k_k \varepsilon_k \left(\prod_i C_i^{\gamma_{i,k}} - K_{sp,k} \right) \right), \tag{3.37}$$

where $\gamma_{i,k}$ is the number of ionic species in precipitate product *k*, k_k is the precipitation rate constant, ε_k is the volume fraction in the cathode, and $K_{sp,k}$ is a solubility product, while subscript *k* is the indicator for precipitate products. The number of ionic species is shared for each precipitate below.

Table 3.5. Number of ionic species for each precipitate.

Species		$\boldsymbol{Li^+}$	$\boldsymbol{S_8^0}$	$\boldsymbol{S_4^{2-}}$	$\boldsymbol{S^{2-}}$	$\boldsymbol{A^-}$
$\boldsymbol{i}$		1	2	3	4	5
$\boldsymbol{\gamma_{i,k}}$	$k=Li_2S_{(s)}$	2	0	0	1	0
	$k=S_{8(s)}$	0	1	0	0	0

The precipitated materials affect the electrolyte volume fraction; it is shown in the equation below:

$$\frac{\partial \varepsilon}{\partial t} = -\sum_k \left(k_k \varepsilon_k \left(\prod_i C_i^{\gamma_{i,k}} - K_{sp,k} \right) \right), \tag{3.38}$$

where $\tilde{V}_k$ is molar volume of precipitate. Also, the volume fraction of precipitates is expressed below,

$$\frac{\partial \varepsilon_k}{\partial t} = \tilde{V}_k R'_k, \tag{3.39}$$

so volume fractions of precipitate will change during discharge.

As previously mentioned, the novel definition of the electrochemically active area is used for this model. The modified version is expressed as,

$$a = a_0 \omega_C \left(\frac{\varepsilon}{\varepsilon_{ref}}\right)^{1.5}. \tag{3.40}$$

In this expression, a_0 is the initial value for the active area, ω_C is the weight fraction of carbon and ε_{ref} is a reference value considering the initial wetting of the cathode.

The model considers the volume fraction of each material, and the total volume fractions are expressed below:

$$\varepsilon_{S_{8(s)}} + \varepsilon_{Li_2S_{(s)}} + \varepsilon_C + \varepsilon_B = 1 - \varepsilon, \tag{3.41}$$

where subscript *B* represents the binder in the cathode.

The current density is expressed by the Butler-Volmer Equation as below:

$$i_j = i_{o,jref}\left\{\prod_i \left(\frac{C_i}{C_{i,ref}}\right)^{p_{i,j}} \exp\left(\frac{\alpha_{aj} \times F}{RT}\eta_j\right) - \prod_i \left(\frac{C_i}{C_{i,ref}}\right)^{q_{i,j}} \exp\left(-\frac{\alpha_{cj} \times F}{RT}\eta_j\right)\right\}. \tag{3.42}$$

In this equation, i_o is reference exchange current density, $C_{i,ref}$ is initial concentration, α is transfer coefficient, p is anodic, and q is cathodic reaction order.

To evaluate the overpotentials, the equation below is used,

$$\eta_j = \phi_s - \phi_e - U_{j,ref}. \tag{3.43}$$

In the equation, ϕ_s is solid phase potential, $U_{j,ref}$ is the open-circuit potential (OCP) of an electrochemical reaction.

For estimating the potentials of the electrochemical reactions, the reversible state of the Nernst equation is used,

$$U_{j,ref} = U_j^0 - \frac{RT}{n_j F}\sum_i s_{i,j} \ln\left(\frac{C_{i,ref}}{1000}\right). \tag{3.44}$$

In this expression, U_j^0 is standard overpotential for the reaction.

The porous electrode theory separates the current density into the liquid/electrolyte and solid phases. While estimating them, different equations are used. The liquid phase current density is expressed by using the diffusion term,

$$i_e = F \sum_i z_i N_i, \tag{3.45}$$

and solid phase current density is expressed by using solid phase potential in Ohm's law,

$$i_s = -\sigma \nabla \phi_s. \tag{3.46}$$

In these expressions, σ represents the conductivity in the cathode.

In addition, electroneutrality is assumed. Hence, the total charges should be zero in the cell. This is shown by the equation below,

$$\sum_i z_i C_i = 0. \tag{3.47}$$

Since this is a 1-D model, governing and boundary conditions are needed to solve the differential equations. The used equations are listed in the following section.

Last but not least, the cell voltage is calculated using solid phase potential at one end of the cathode and liquid phase potential at the other end of the cathode. It is expressed as below,

$$E_{cell} = \phi_s(L) - \phi_e(0). \tag{3.48}$$

3.2.1. Governing Equations

Below are the governing equations used in the model.

$$\frac{\partial \varepsilon C_{Li^+}}{\partial t} = -\frac{\partial}{\partial x}\left(-\left(D_{Li^+,0}\varepsilon^b\right)\frac{\partial C_{Li^+}}{\partial x} - z_{Li^+}\frac{\left(D_{Li^+,0}\varepsilon^b\right)}{RT}FC_{Li^+}\frac{\partial \phi_e}{\partial x}\right) - \gamma_{Li^+,Li_2S}\left(k_{Li_2S}\varepsilon_{Li_2S}\left(\left(C_{Li^+}^{\gamma_{Li^+,Li_2S}}\right)\left(C_{S^{2-}}^{\gamma_{S^{2-},Li_2S}}\right) - K_{sp,Li_2S}\right)\right) \tag{3.49}$$

$$\frac{\partial \varepsilon C_{S_8^0}}{\partial t} = -\frac{\partial}{\partial x}\left(-\left(D_{S_8^0,0}\varepsilon^b\right)\frac{\partial C_{S_8^0}}{\partial x} - z_{S_8^0}\frac{\left(D_{S_8^0,0}\varepsilon^b\right)}{RT}FC_{S_8^0}\frac{\partial \phi_e}{\partial x}\right) + \left(-a_0\left(\frac{\varepsilon}{\varepsilon_{initial}}\right)^{\xi}\left(\frac{\frac{-1}{4}i_1}{F}\right)\right) - \gamma_{S_8^0,S_{8(s)}}\left(k_{S_{8(s)}}\varepsilon_{S_{8(s)}}\left(\left(C_{S_8^0}^{\gamma_{S_8^0,S_{8(s)}}}\right) - K_{sp,S_{8(s)}}\right)\right) \tag{3.50}$$

$$\frac{\partial \varepsilon C_{S_4^{2-}}}{\partial t} = -\frac{\partial}{\partial x}\left(-\left(D_{S_4^{2-},0}\varepsilon^b\right)\frac{\partial C_{S_4^{2-}}}{\partial x} - z_{S_4^{2-}}\frac{\left(D_{S_4^{2-},0}\varepsilon^b\right)}{RT}FC_{S_4^{2-}}\frac{\partial \phi_e}{\partial x}\right) + \left(-a_0\left(\frac{\varepsilon}{\varepsilon_{initial}}\right)^{\xi}\left(\frac{\frac{1}{2}i_1 - \frac{1}{6}i_2}{F}\right)\right) \tag{3.51}$$

$$\frac{\partial \varepsilon C_{S^{2-}}}{\partial t} = -\frac{\partial}{\partial x}\left(-\left(D_{S^{2-},0}\varepsilon^b\right)\frac{\partial C_{S^{2-}}}{\partial x} - z_{S^{2-}}\frac{\left(D_{S^{2-},0}\varepsilon^b\right)}{RT}FC_{S^{2-}}\frac{\partial \phi_e}{\partial x}\right) + \left(-a_0\left(\frac{\varepsilon}{\varepsilon_{initial}}\right)^{\xi}\left(\frac{\frac{2}{3}i_2}{F}\right)\right) - \gamma_{S^{2-},Li_2S}\left(k_{Li_2S}\varepsilon_{Li_2S}\left(\left(C_{Li^+}^{\gamma_{Li^+,Li_2S}}\right)\left(C_{S^{2-}}^{\gamma_{S^{2-},Li_2S}}\right) - K_{sp,Li_2S}\right)\right) \tag{3.52}$$

$$C_{A^-} = C_{Li^+} - 2C_{S_4^{2-}} - 2C_{S^{2-}} \tag{3.53}$$

$$i_1 = i_{0,1ref}\left\{\left(\frac{C_{S_4^{2-}}}{C_{S_4^{2-},ref}}\right)^{\frac{1}{2}}\exp\left(\frac{\alpha_{a_1}F}{RT}\eta_1\right) - \left(\frac{C_{S_8^0}}{C_{S_8^0,ref}}\right)^{\frac{1}{4}}\exp\left(\frac{-\alpha_{c_1}F}{RT}\eta_1\right)\right\} \tag{3.54}$$

$$i_2 = i_{0,2ref}\left\{\left(\frac{C_{S^{2-}}}{C_{S^{2-},ref}}\right)^{\frac{2}{3}}\exp\left(\frac{\alpha_{a_2}F}{RT}\eta_2\right) - \left(\frac{C_{S_4^{2-}}}{C_{S_4^{2-},ref}}\right)^{\frac{1}{6}}\exp\left(\frac{-\alpha_{c_2}F}{RT}\eta_2\right)\right\} \tag{3.55}$$

$$i_s = -\sigma\frac{\partial \phi_s}{\partial x} \tag{3.56}$$

$$i_e = F\left(\left(z_{Li^+}\left(-\left(D_{Li^+,0}\varepsilon^b\right)\frac{\partial C_{Li^+}}{\partial x} - z_{Li^+}\frac{\left(D_{Li^+,0}\varepsilon^b\right)}{RT}FC_{Li^+}\frac{\partial \phi_e}{\partial x}\right)\right) + \left(z_{S_8^0}\left(-\left(D_{S_8^0,0}\varepsilon^b\right)\frac{\partial C_{S_8^0}}{\partial x} - z_{S_8^0}\frac{\left(D_{S_8^0,0}\varepsilon^b\right)}{RT}FC_{S_8^0}\frac{\partial \phi_e}{\partial x}\right)\right) + \left(z_{S_4^{2-}}\left(-\left(D_{S_4^{2-},0}\varepsilon^b\right)\frac{\partial C_{S_4^{2-}}}{\partial x} - z_{S_4^{2-}}\frac{\left(D_{S_4^{2-},0}\varepsilon^b\right)}{RT}FC_{S_4^{2-}}\frac{\partial \phi_e}{\partial x}\right)\right) + \left(z_{S^{2-}}\left(-\left(D_{S^{2-},0}\varepsilon^b\right)\frac{\partial C_{S^{2-}}}{\partial x} - z_{S^{2-}}\frac{\left(D_{S^{2-},0}\varepsilon^b\right)}{RT}FC_{S^{2-}}\frac{\partial \phi_e}{\partial x}\right)\right) + \left(z_{A^-}\left(-\left(D_{A^-,0}\varepsilon^b\right)\frac{\partial C_{A^-}}{\partial x} - z_{A^-}\frac{\left(D_{A^-,0}\varepsilon^b\right)}{RT}FC_{A^-}\frac{\partial \phi_e}{\partial x}\right)\right)\right) \tag{3.57}$$

$$I_{app} = i_e + i_s \tag{3.58}$$

$$\frac{\partial i_e}{\partial x} = a(i_1 + i_2) \tag{3.59}$$

$$\frac{\partial \varepsilon}{\partial t} = -\left(\tilde{V}_{Li_2S_{(s)}}k_{Li_2S}\varepsilon_{Li_2S}\left(\left(C_{Li^+}^{\gamma_{Li^+,Li_2S}}\right)\left(C_{S^{2-}}^{\gamma_{S^{2-},Li_2S}}\right) - K_{sp,Li_2S}\right) + \tilde{V}_{S_{8(s)}}k_{S_{8(s)}}\varepsilon_{S_{8(s)}}\left(\left(C_{S_8^0}^{\gamma_{S_8^0,S_{8(s)}}}\right) - K_{sp,S_{8(s)}}\right)\right) \tag{3.60}$$

$$\frac{\partial \varepsilon_{Li_2S_{(s)}}}{\partial t} = \tilde{V}_{Li_2S_{(s)}}k_{Li_2S}\varepsilon_{Li_2S}\left(\left(C_{Li^+}^{\gamma_{Li^+,Li_2S}}\right)\left(C_{S^{2-}}^{\gamma_{S^{2-},Li_2S}}\right) - K_{sp,Li_2S}\right) \tag{3.61}$$

$$\varepsilon_{S_{8(s)}} = 1 - \varepsilon - \varepsilon_{Li_2S_{(s)}} - \varepsilon_C - \varepsilon_B. \tag{3.62}$$

3.2.2. Boundary Conditions

When $x = 0$, these boundary conditions are used.

$$C_{Li^+} = C_{Li^+_{ref}} \tag{3.63}$$

$$C_{S_8^0} = C_{S_8^0{}_{ref}} \tag{3.64}$$

$$C_{S_4^{2-}} = C_{S_4^{2-}{}_{ref}} \tag{3.65}$$

$$C_{S^{2-}} = C_{S^{2-}{}_{ref}} \tag{3.66}$$

$$C_{A^-} = C_{A^-_{ref}} \tag{3.67}$$
$$\phi_s = 0 \tag{3.68}$$
$$i_s = 0 \tag{3.69}$$
$$i_e = I_{app}. \tag{3.70}$$

When $x = L$, these boundary conditions are used.

$$N_{Li^+} = 0 \tag{3.71}$$
$$N_{S_8^0} = 0 \tag{3.72}$$
$$N_{S_4^{2-}} = 0 \tag{3.73}$$
$$N_{S^{2-}} = 0 \tag{3.74}$$
$$N_{A^-} = 0 \tag{3.75}$$
$$i_s = I_{app} \tag{3.76}$$
$$i_e = 0. \tag{3.77}$$

3.2.3. Initial Conditions

The initial conditions below are used in the model by Abdulkadiroglu, Bektas, and Eroglu [8]:

$$C_{Li^+} = C_{Li^+_{ref}} \tag{3.78}$$
$$C_{S_8^0} = C_{S_8^0{}_{ref}} \tag{3.79}$$
$$C_{S_4^{2-}} = C_{S_4^{2-}{}_{ref}} \tag{3.80}$$
$$C_{S^{2-}} = C_{S^{2-}{}_{ref}} \tag{3.81}$$
$$C_{A^-} = C_{A^-_{ref}} \tag{3.82}$$
$$i_1 = -\frac{I_{app}}{a_0 L} \tag{3.83}$$
$$i_2 = 0 \tag{3.84}$$
$$\phi_s = -\frac{I_{app}}{2\sigma L}x^2 \tag{3.85}$$
$$\phi_e = \phi_s - U_{1,ref} + \frac{RT}{a_c F}\ln\left(\frac{I_{app}}{a_0 L i_{0,1_{ref}}}\right) \tag{3.86}$$
$$i_s = I_{app} - i_e \tag{3.87}$$
$$i_e = I_{app}\left(1 - \frac{x}{L}\right) \tag{3.88}$$
$$\varepsilon = \varepsilon_{initial} \tag{3.89}$$

$$\varepsilon_{Li_2S_{(s)}} = \varepsilon_{Li_2S_{(s)}{}_{initial}} \quad (3.90)$$

$$\varepsilon_{S_{8(s)}} = \varepsilon_{S_{8(s)}{}_{initial}}. \quad (3.91)$$

3.2.4. Parameters in the Model

The parameters in the model are shared below.

Table 3.6. Cell parameters for the one-dimensional model.

Notation	Name	Units	Value
U_1^0	Standard potential of high voltage plateau	V	2.3
U_2^0	Standard potential of low voltage plateau	V	2.0
$i_{0,1_{ref}}$	Exchange current density of first electrochemical reaction	A m^{-2}	$0.8x10^{-2}$
$i_{0,2_{ref}}$	Exchange current density of second electrochemical reaction	A m^{-2}	$1x10^{-2}$
T	Temperature	K	298
σ	Electronic conductivity of cathode	S m^{-1}	1.0

Table 3.7. Cell parameters for the one-dimensional model. (cont.)

Notation	Name	Units	Value
α_a, α_c	Anodic and cathodic charge transfer coefficients	-	0.5
a_0	Initial specific surface area of the cathode	$m^2\ m^{-3}$	796572
$D_{Li^+,0}$	Diffusion coefficient of Li^+	$m^2\ s^{-1}$	$0.85x10^{-12}$
$D_{S_8^0,0}$	Diffusion coefficient of S_8^0	$m^2\ s^{-1}$	$2.0x10^{-11}$
$D_{S_4^{2-},0}$	Diffusion coefficient of S_4^{2-}	$m^2\ s^{-1}$	$2.0x10^{-12}$
$D_{S^{2-},0}$	Diffusion coefficient of S^{2-}	$m^2\ s^{-1}$	$2.0x10^{-12}$
$D_{A^-,0}$	Diffusion coefficient of A^-	$m^2\ s^{-1}$	$8.0x10^{-12}$
$C_{Li^+_{ref}}$	Reference concentration of Li^+	$mol\ m^{-3}$	850.88
$C_{S_8^0{}_{ref}}$	Reference concentration of S_8^0	$mol\ m^{-3}$	1.9
$C_{S_4^{2-}{}_{ref}}$	Reference concentration of S_4^{2-}	$mol\ m^{-3}$	0.02
$C_{S^{2-}{}_{ref}}$	Reference concentration of S^{2-}	$mol\ m^{-3}$	$8.267x10^{-10}$

Table 3.8. Cell parameters for the one-dimensional model. (cont.)

Notation	Name	Units	Value
$C_{A^-_{ref}}$	Reference concentration of A^-	mol m^{-3}	1000
$k_{Li_2S_{(s)}}$	Rate constant of precipitation of species $Li_2S_{(s)}$	m^6 mol^2 s^{-1}	137.5x10^{-5}
$k_{S_{8(s)}}$	Rate constant of precipitation of species $S_{8(s)}$	s^{-1}	10
$K_{sp,Li_2S_{(s)}}$	Solubility product of precipitate $Li_2S_{(s)}$	mol^3 m	3.0x10^{-3}
$K_{sp,S_{8(s)}}$	Solubility product of precipitate $S_{8(s)}$	mol m^3	19
$\tilde{V}_{Li_2S_{(s)}}$	Molar volume of precipitate $Li_2S_{(s)}$	m^3 mol	2.4x10^{-5}
$\tilde{V}_{S_{8(s)}}$	Molar volume of precipitate $S_{8(s)}$	m^3 mol	1.239x10^{-4}

3.2.5. Cell Design Parameters

To determine the specifications of cathode volume and mass fractions, we used the equations below:

$$\varepsilon_C = 1 - \varepsilon - \varepsilon_{S_{8(s)}} - \varepsilon_{Li_2S_{(s)}} - \varepsilon_B \quad (3.92)$$

$$\omega_C = 1 - \omega_S - \omega_B. \quad (3.93)$$

On the other hand, the applied current is estimated in terms of the C-rate. The equation used is shared herein:

$$I_{app} = Sulfur\ loading \times\ C - rate. \quad (3.94)$$

Table 3.9. Cell design parameters for the one-dimensional model.

Notation	Name	Units	Value
E/S ratio	Electrolyte volume to Sulfur mass ratio	mL g^{-1} Sulfur	20.56
C/S ratio	Carbon to Sulfur weight ratios	-	1.2
ω_S	Cathode sulfur weight fraction	-	0.41
ω_C	Cathode carbon weight fraction	-	0.49
ω_B	Cathode binder weight fraction	-	0.1
ρ_S	Sulfur density	g cm^{-3}	2.07
ρ_C	Carbon density	g cm^{-3}	1.8
ρ_B	Binder density	g cm^{-3}	1.77
$\rho_{Electrolyte}$	Electrolyte density	g cm^{-3}	1.2
$\rho_{Cathode}$	Cathode density	g cm^{-3}	$1.12x10^{-1}$
$\varepsilon_{S_{8(s)}}$	Cathode sulfur volume fraction	-	$2.21x10^{-2}$
ε_C	Cathode carbon volume fraction	-	$3.05x10^{-2}$
ε_B	Cathode binder volume fraction	-	5.32x10-3
$\varepsilon_{initial}$	Initial cathode porosity	-	0.941

Table 3.10. Cell design parameters for the one-dimensional model. (cont.)

Notation	Name	Units	Value
$\varepsilon_{Li_2S_{(s)}}$	Cathode $Li_2S_{(s)}$ volume fraction	-	0.001
ε_{ref}	Reference cathode porosity	-	0.99
L	Cathode thickness	m	2.25×10^{-4}
-	Sulfur loading	mg cm^{-2}	1.030
I_{app}	Applied current density	mA m^{-2}	17.25

The mentioned parameters are used during the sensitivity analysis. Some parameters are revised to understand the effect of the C/S ratio and S loading. The mentioned parameters are used to determine the cell design parameters. The equations are shared herein:

$$\text{E/S ratio} = \frac{\varepsilon_{initial}}{\varepsilon_{S_{8_{(s)}}} \rho_S} \tag{3.95}$$

$$\text{C/S ratio} = \frac{\omega_C}{\omega_S} \tag{3.96}$$

$$\text{S loading} = L\rho_{Cathode}\omega_S. \tag{3.97}$$

While changing the C/S ratio to vary the S loading in the cell, the E/S ratio and cathode thickness remain constant. The following parameters are used in this analysis.

Table 3.11. Cell design parameters used for the C/S variation cases.

Notation	Units	Value										
		1	2	3	4	5	6	7	8	9	10	11
E/S ratio	mL g^{-1} Sulfur	21	21	21	21	21	21	21	21	21	21	21

Table 3.12. Cell design parameters used for the C/S variation cases. (cont.)

Notation	Units	Value										
		1	2	3	4	5	6	7	8	9	10	11
C/S ratio	-	1	2	3	4	5	6	7	8	9	10	11
ω_S	-	0.69	0.60	0.53	0.45	0.41	0.36	0.33	0.30	0.23	0.15	0.10
ω_C	-	0.21	0.30	0.68	0.45	0.49	0.54	0.57	0.60	0.68	0.75	0.80
$\varepsilon_{S_{8(s)}}$	-	2.27 x10^{-2}	2.26 x10^{-2}	2.22 x10^{-2}	2.22 x10^{-2}	2.21x 10^{-2}	2.19 x10^{-2}	2.18 x10^{-2}	2.16 x10^{-2}	2.10 x10^{-2}	2.00 x10^{-2}	1.85 x10^{-2}
ε_C	-	7.83 x10^{-3}	1.30 x10^{-2}	1.81x 10-2	2.56 x10^{-2}	3.05x 10^{-2}	3.78 x10^{-2}	4.26 x10^{-2}	4.97 x10^{-2}	7.26 x10^{-2}	1.15 x10^{-1}	1.71 x10^{-1}
ε_B	-	2.83 x10^{-3}	3.40 x10^{-3}	3.96 x10^{-3}	4.78 x10^{-3}	5.32x 10^{-3}	6.13 x10^{-3}	6.65 x10^{-3}	7.43 x10^{-3}	9.94 x10^{-3}	1.46 x10^{-3}	2.07 x10^{-3}
$\varepsilon_{initial}$	-	0.97	0.96	0.96	0.95	0.94	0.93	0.93	0.92	0.90	0.85	0.79
L	m	2.25 x10^{-4}	2.25 x10^{-4}	2.25 x10^{-4}	2.25 x10^{-4}	2.25 x10^{-4}	2.25 x10^{-4}	2.25 x10^{-4}	2.25 x10^{-4}	2.25 x10^{-4}	2.25 x10^{-4}	2.25 x10^{-4}
Sulfur loading	mg cm^{-2}	1.06	1.05	1.045	1.036	1.030	1.02	1.02	1.01	0.98	0.93	0.86
I_{app}	mA m^{-2}	17.71	17.60	17.50	17.35	17.25	17.11	17.01	16.87	16.42	15.58	14.47

On the other hand, the S loading in the cathode is also changed by changing the cathode thickness while keeping the E/S and C/S ratios constant. So, the thickness of the cell is increased with increasing sulfur content. The parameters used in this analysis are given below.

Table 3.13. Cell design parameters used for the cathode thickness variation cases.

Notation	Units	Value					
		1	2	3	4	5	6
E/S ratio	mL g^{-1} Sulfur	21	21	21	21	21	21
C/S ratio	-	1.2	1.2	1.2	1.2	1.2	1.2
ω_S	-	0.41	0.41	0.41	0.41	0.41	0.41
ω_C	-	0.49	0.49	0.49	0.49	0.49	0.49
$\varepsilon_{S_{8(s)}}$	-	2.21x10^{-2}	2.21x10^{-2}	2.21x10^{-2}	2.21x10^{-2}	2.21x10^{-2}	2.21x10^{-2}
ε_C	-	3.05x10^{-2}	3.05x10^{-2}	3.05x10^{-2}	3.05x10^{-2}	3.05x10^{-2}	3.05x10^{-2}
ε_B	-	5.32x10^{-3}	5.32x10^{-3}	5.32x10^{-3}	5.32x10^{-3}	5.32x10^{-3}	5.32x10^{-3}
$\varepsilon_{initial}$	-	0.94	0.94	0.94	0.94	0.94	0.94
L	m	2.00 x10^{-4}	2.25 x10^{-4}	2.50 x10^{-4}	3.00 x10^{-4}	5.00 x10^{-4}	8.00 x10^{-4}
Sulfur loading	mg cm^{-2}	0.915	1.030	1.144	1.373	2.289	3.662
I_{app}	mA m^{-2}	15.33	17.25	19.17	23.00	38.34	61.34

3.3. Linearization Procedure

The differential equations are linearized for a tridiagonal matrix algorithm. All governing equations are linearized to be expressed as below:

$$a_{i,k}(x)\frac{d^2C_k}{dx^2} + b_{i,k}(x)\frac{dC_k}{dx} + d_{i,k}(x)C_k = g_i(x). \tag{3.98}$$

In this expression, *a, b, d,* and *g* are functions in the differential equations. Also, subscript *i* represents the differential equation that needs to be solved, and *k* represents the variables in the model.

The boundary equations are linearized as below:

$$p_{i,k}(x)\frac{dC_k}{dx} + e_{i,k}(x)C_k = f_i, \tag{3.99}$$

where *p* and *e* are functions in differential equations. With the help of the Taylor series approximation, we can apply the linearization procedure to the model. The Taylor series approximation is shown below if f(x) at t=x is known,

$$f(x) = f(a) + f'(a)f(x-a). \tag{3.100}$$

For example, Equation (3.13) is linearized, such as below,

$$\frac{dS_8^0}{dt} + k_s S_8^0 + \frac{n_{S_8} M_{S_8}}{n_e F} i_H = \frac{\Delta S_8^0}{\Delta t} + k_s S_8^0 + \frac{n_{S_8} M_{S_8}}{n_e F} i_H, \tag{3.101}$$

and the equation is multiplied by Δt;

$$\Delta S_8^0 + k_s \Delta t \left(S_{8_{\text{prev}}}^0 + \Delta S_8^0\right) + \frac{n_{S_8} M_{S_8}}{n_e F}\Delta t(i_{H_{prev}} + \Delta i_H) = 0 \tag{3.102}$$

$$\Delta S_8^0(1 + k_s\Delta t) + \frac{n_{S_8} M_{S_8}}{n_e F}\Delta t(\Delta i_H) = -\left(S_{8_{\text{prev}}}^0 k_s \Delta t\right) - \frac{n_{S_8} M_{S_8}}{n_e F}\Delta t i_{H_{prev}}. \tag{3.103}$$

Now, the linearization procedure is applicable;

$$d_{1,1} = 1 + k_s\Delta t \tag{3.104}$$

$$d_{1,6} = \frac{n_{S_8} M_{S_8}}{n_e F}\Delta t \tag{3.105}$$

$$g_1 = -\left(S_{8_{\text{prev}}}^0 k_s \Delta t\right) - \frac{n_{S_8} M_{S_8}}{n_e F}\Delta t i_{H_{prev}} \tag{3.106}$$

In addition, please note that nonlinear terms are neglected, such as, $(\Delta S_8^0 \Delta i_H)$.

4. RESULTS AND DISCUSSIONS

The sensitivity and sulfur loading analysis results are shared in this part for the aforementioned electrochemical models. The voltage curve of a Li-S cell is studied and compared to analyze the variables' effect on the capacity and voltage. The selected electrochemical models estimate discharge performances up to a dramatic voltage drop due to species change. The discharge profile then ends because the model cannot predict further.

The design parameters are those that can be controlled experimentally. The sensitivity analysis, however, considers the effect of assumed parameters such as transport and reaction kinetics. Thus, the design parameters are considered separately from the sensitivity analysis.

4.1. Zero-Dimensional Electrochemical Model

4.1.1. Predictions of the S Loading Effect on the Discharge Performance

Sulfur loading is a crucial cell design parameter for the performance and capacity of *Li-S* batteries [24,25]. As discussed earlier, our aim in this thesis is to study the effectiveness of a zero-dimensional model in predicting the impact of the S loading on the discharge performance of a Li-S cell. The model is not flexible in defining the cathode design parameters, such as the cathode's carbon mass or the cathode's thickness. However, sulfur mass can be varied; as seen in Figure 4.1, we changed the S mass between 0.7g and 10g per cell for this purpose. The model does not consider the geometric cell area; therefore, the impact of S mass rather than the S loading is discussed here.

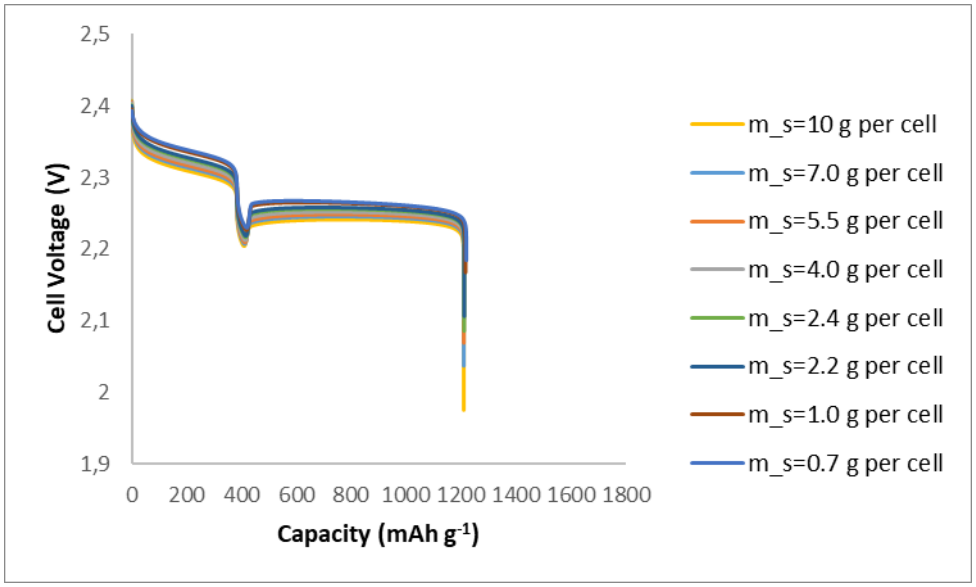

Figure 4.1. Discharges profile for different sulfur masses at 1C.

Elevated voltage plateaus are observed from the voltage curve, Figure 4.1, with decreasing S loading, but no significant capacity change is observed. The applied current for 1C-rate is different in each case; this can be the reason for such voltage elevation as the applied current is lower for lower S loadings.

The predicted voltage curves do not show a capacity change with sulfur loading variation. The expectation from the experimental results is that the S loading should significantly affect cell performance and discharge capacity [4].

When S loading is high, the electrolyte becomes more concentrated. Because of the high polysulfide concentration, one of the adverse effects is ionic transport. Due to high polarization, ionic transport can be slower, hindering the kinetics. Another reason is the decrease in conductivity; since sulfur is an insulator material, the cathode conductivity decreases with the high sulfur amount. Another effect is the precipitation rate of polysulfides; more precipitated material can be produced in the saturated electrolyte. As a result, more precipitated material forms at the cathode surface, and they decrease the active cathode area. Similarly, the applied current at a given C-rate increases with increasing S loading expected also to reduce the capacity. Therefore, we should expect a significant change in the discharge performance by S loading variation. Hence, we can say that the

model is not sensitive to sulfur mass and cannot capture the S-loading effect on the discharge capacity. To investigate the model's limits and whether the effect of S loading on the discharge capacity can be predicted implicitly through a model parameter, we conducted a detailed sensitivity analysis on the model, as discussed next.

4.1.2. Sensitivity Results

In this section, the sensitivity analysis is presented first. During the study, various parameters are changed, and the performance response is observed via the voltage curve. Each parameter affects the performance differently. Hence, the results are obtained and shared individually.

4.1.2.1. Active Area. The model defines the reaction kinetics using the Butler-Volmer equation, including the active area. Therefore, we expect the active area to affect the cell performance. The voltage curves obtained when the active area is ten times higher and ten times lower than the reference value are shared below. So the modification changed the kinetics of the high- and low-voltage plateaus. Both voltage plateaus are affected, which is expected because both reaction kinetics similarly include the active area term, e.g., Equations (3.7)-(3.8). In other words, the high and low-voltage curves are influenced in the same way. When it gets higher, the exposure area for the electrochemical reactions will be higher; therefore, this modification will increase the reaction rate and voltage output. The same phenomena can explain the opposite case. However, as seen in the figure, the active area does not affect the capacity.

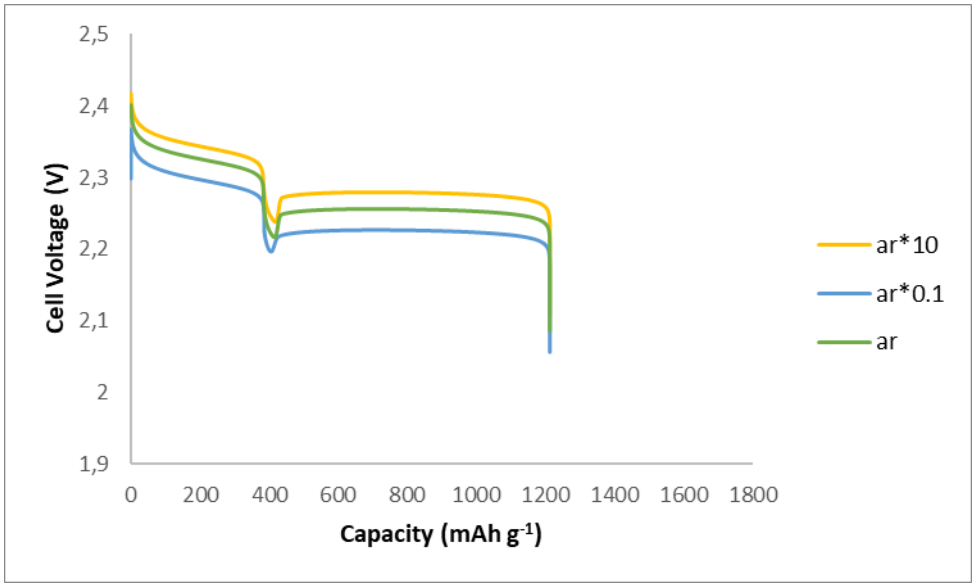

Figure 4.2. Discharge profiles for different active areas at 1C.

In the literature, various studies investigate the importance of the active area in the cathode [7,19]. The previous results show that the active area changes during discharge due to precipitation reactions. Since the model keeps the active area constant and independent of the cathode porosity, its effect on the capacity is limited.

4.1.2.2. Initial Cell Voltage. The simulation starts with an initial assumption for the cell voltage, then Nernst potentials and overpotentials are estimated for the voltage plateaus. Therefore, the initial value is changed to understand the response in this sensitivity analysis.

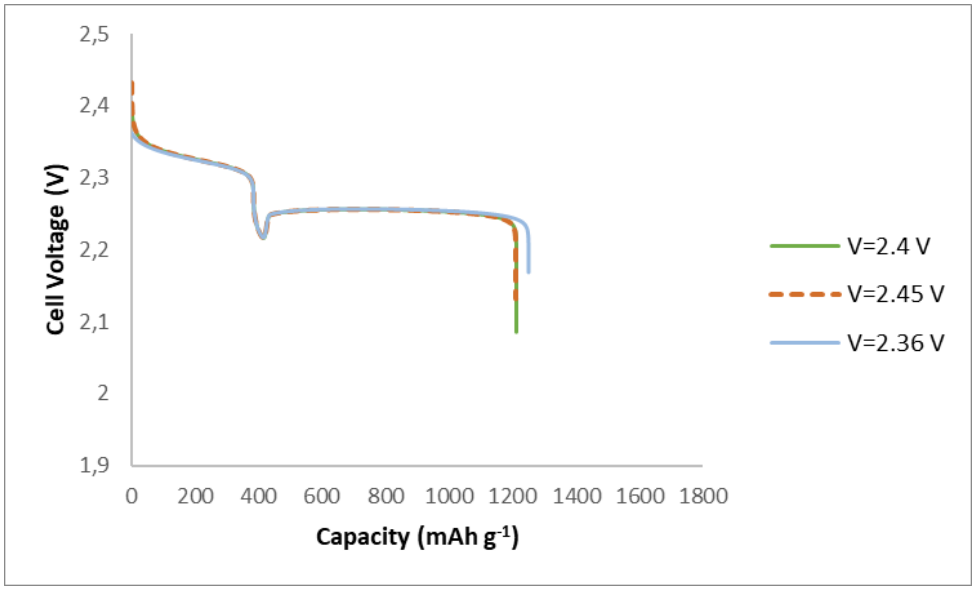

Figure 4.3. Discharge profiles for different initial voltages at 1C.

The voltage curve is obtained when the initial cell voltage is 2.45 V and 2.36 V. It can be seen in the figure that the change in the initial voltage value has a slight effect only at the beginning of the high voltage plateau. This initial shift is expected because the model uses the initial voltage value to estimate the equilibrium potentials for the voltage plateaus. The second voltage plateau remains unchanged. During discharge, the equilibrium potentials are estimated by the Butler-Volmer equations simultaneously. The effect of the initial voltage can be minimized or canceled before the second reaction starts. When the initial voltage is high, the Nernst overpotential will be higher. Therefore, the model estimates a faster first reaction. More S_8^0 mass undergoes the reduction reaction by contributing to the current. On the other hand, unexpectedly, there is a slight capacity decrease with a change in the initial value.

4.1.2.3. Standard Potentials for High and Low Voltage Plateaus. As mentioned earlier, the driving force for the electrochemical reactions is related to the Nernst potentials. The model estimates Nernst potentials using equilibrium potentials, which are also estimated by standard potentials. So, this section changes standard potentials for the high and low voltage plateaus, and the cell response is analyzed.

Figure 4.4 shows the discharge curve of the model when the standard potential for high voltage plateau is multiplied by a factor of 1.03 and 0.95.

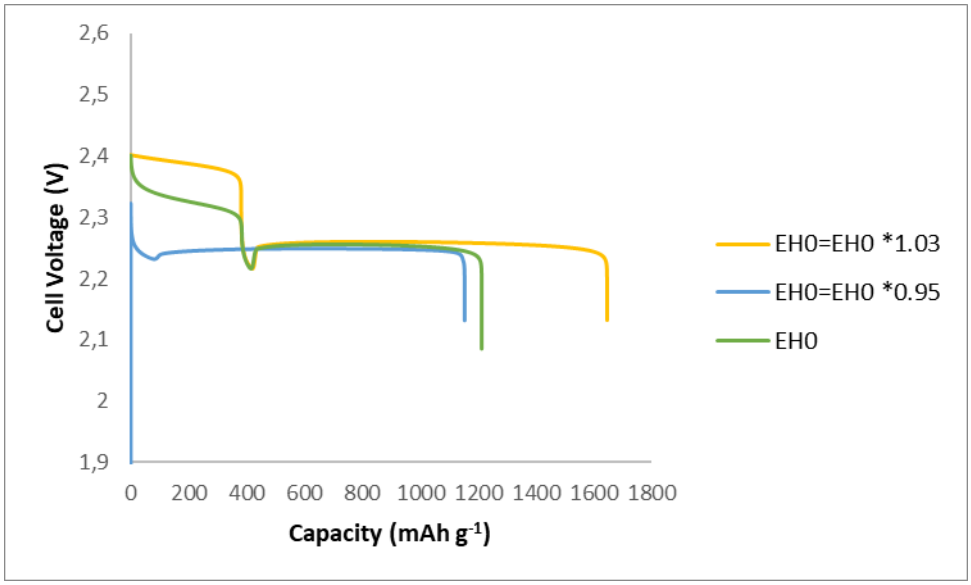

Figure 4.4. Discharge profiles for different high equilibrium potentials at 1C.

When the standard potential is higher, the high-voltage plateau is elevated. We can understand that the first reaction kinetics are positively affected as the high-voltage plateau becomes flatter and the low-voltage plateau is extended, causing a capacity increase. In the other case, when the gap between the standard potentials closes, the high voltage plateau becomes unrecognizable. Therefore, the sequence of the multi-step reactions can be disrupted and hurt sulfur utilization.

Figure 4.5 shows the predicted discharge curve when the standard potential for the low voltage plateau is multiplied by a factor of 1.05 and 0.95.

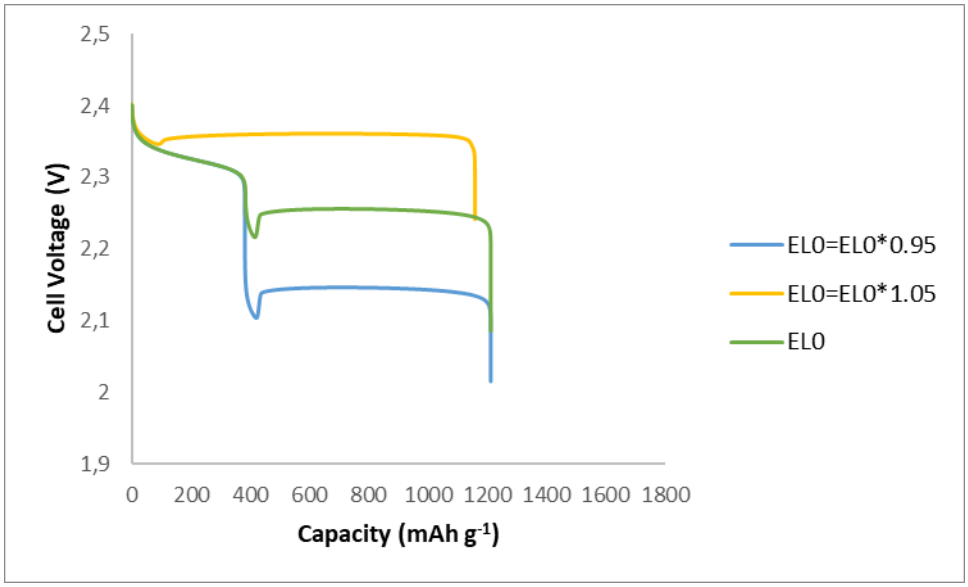

Figure 4.5. Discharge profiles for different low equilibrium potentials at 1C.

As expected, we observe that the two plateaus get less distinguishable as we increase the standard potential for the low-voltage plateau. Similarly, a more distinct jump in the voltage is observed in the opposite case. On the other hand, unlike in Figure 4.4, changing E^0_L does not significantly affect the total capacity. Both standard potentials significantly affect the voltage dip between the voltage plateaus.

4.1.2.4. Exchange Current Densities. In the model, the exchange current density is an effective parameter of the electrochemical reaction rate, so the exchange current densities are also changed and analyzed individually for this study.

The exchange current density for the first reaction is multiplied by a factor of 0.1 and 5 for the analysis. The voltage curves are compared for those values.

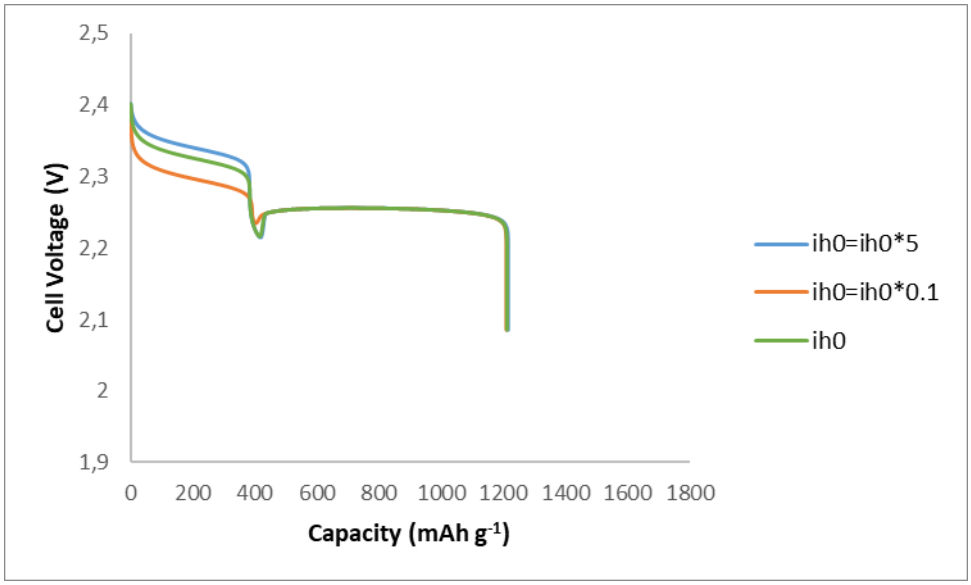

Figure 4.6. Discharge profiles for different high exchange current densities at 1C.

From Figure 4.6, we understand that the exchange current density for the first reaction does not cause a significant change in the low plateau, as expected. On the other hand, the voltage shift is recognizable in the high plateau. When the reactions are fast, the current contribution from the electrochemical reactions will be higher. Therefore, the high-voltage plateau is elevated due to high reaction rates. We can see the opposite effect when the exchange current density is reduced.

When the exchange current density is ten times higher and lower for the second reaction, the voltage curves taken from the simulation are shared below.

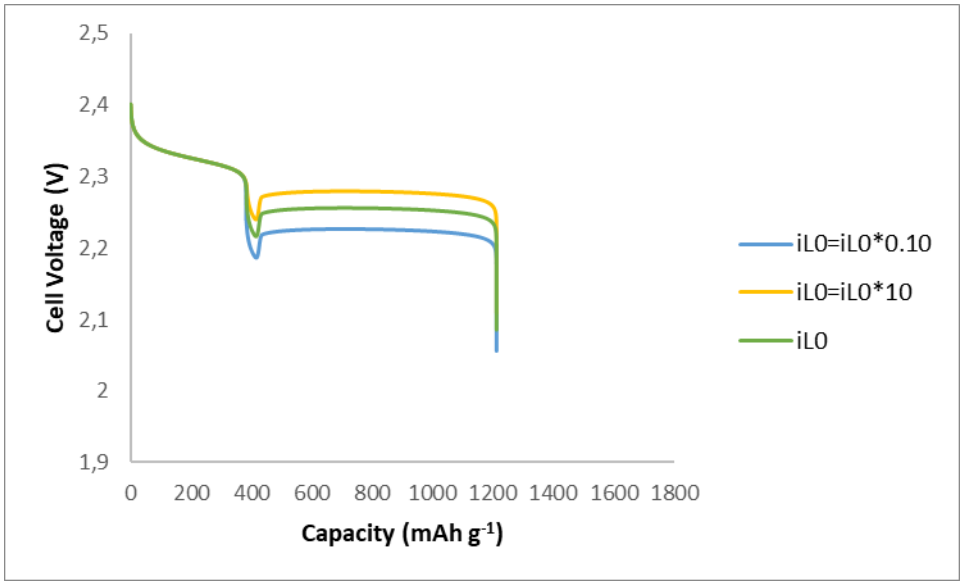

Figure 4.7. Discharge profiles for different low exchange current densities at 1C.

So the voltage shift is expected in the low plateau region. The overpotential of the reduction reaction becomes lower when the exchange current density is higher and vice versa.

For the two parameters, any effect on the capacity is not observed. The study by Ghaznavi and Chen [12] provides information on these parameters, although the study is conducted on the model by Kumaresan et al. [1]. The study shows that reaction kinetics may cause capacity loss depending on the reduction reaction. Also, the reduction reactions occur in sequence, so a chain effect can be expected. However, in this simplified model, we cannot observe these phenomena.

4.1.2.5. Precipitation Rate and Shuttle Constant. This simple model aims to capture the effect of precipitation and shuttle mechanisms on cell behavior through a precipitation rate constant and a shuttle constant. Therefore these two parameters are essential and included in the sensitivity analysis.

The precipitation rate is multiplied and divided by ten to compare the obtained voltage curves.

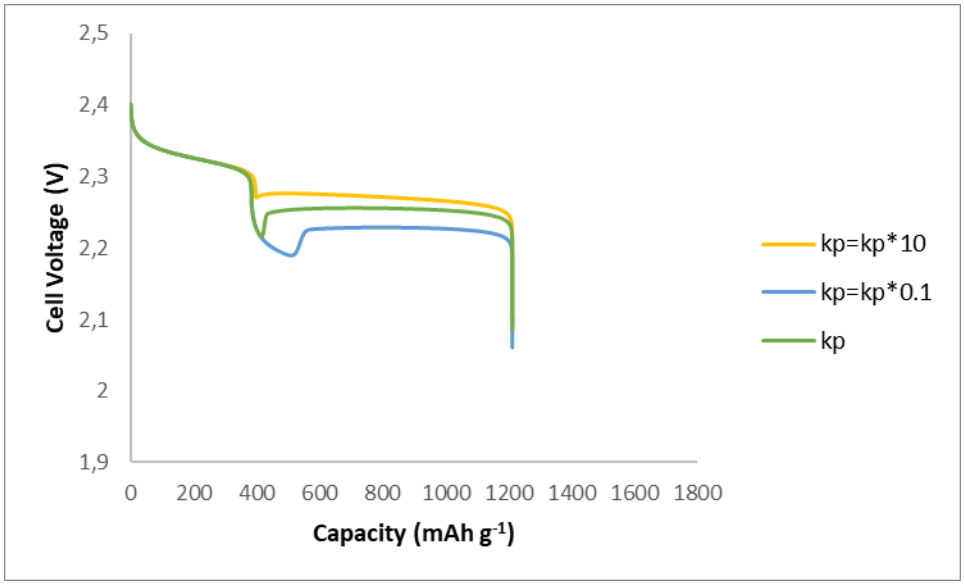

Figure 4.8. Discharge profiles for different precipitation constants at 1C.

The voltage dip between the two voltage plateaus is known to occur when the precipitation of the discharge product first starts. Consequently, k_p has a noticeable impact on the voltage dip on the curve, as shown in Figure 4.8. When the precipitation rate is higher, the dissolved S^{2-} in the electrolyte will be less. So, the model estimates that the second reaction will be driven forward. More S_4^{2-} will be consumed, and the second reaction will occur earlier. The opposite explanation can be valid for the lower precipitation value. No capacity effect is observed from the variation of this parameter. However, a capacity loss is expected when the precipitation rate is increased. The sulfur utilization is expected to be lower in the electrochemical reactions when the precipitation rate is higher. However, this trend is not captured by the model. The study by Ghaznavi and Chen [11] shows that precipitation rates are effective parameters for the response of the cell and its capacity. The model does not include any porosity change in the cathode due to precipitation, so we cannot observe any capacity change with changing model parameters.

Next, the shuttle constant is multiplied and divided by a factor of 10, and the voltage curves are shared in Figure 4.9.

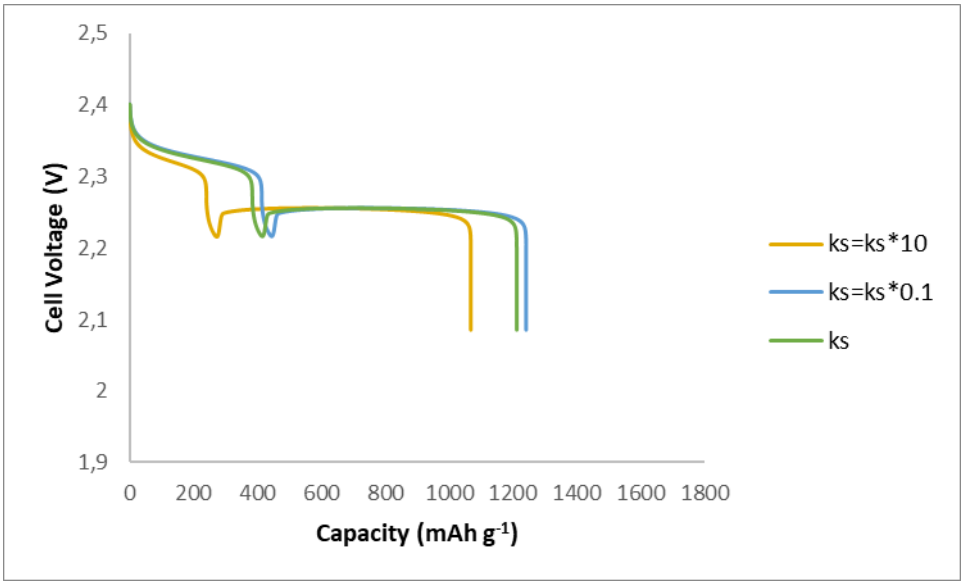

Figure 4.9. Discharge profiles for different shuttle constants at 1C.

The model uses this constant to estimate the rate of the polysulfide shuttle. When the shuttle rate is high, more dissolved sulfur is consumed without contributing to the current. The loss of the active material can lead to a limited high-voltage plateau, as seen in the figure. When the rate is low, more active material will be available for the electrochemical reactions, and a more extended voltage plateau can be observed. Although the effect on the low voltage plateau capacity is insignificant, there is a capacity change due to the extended or limited high voltage plateau.

4.1.2.6. C-rate. The simulated cell voltage curves at 1.5C, 1C, and C/2 are shared in Figure 4.10.

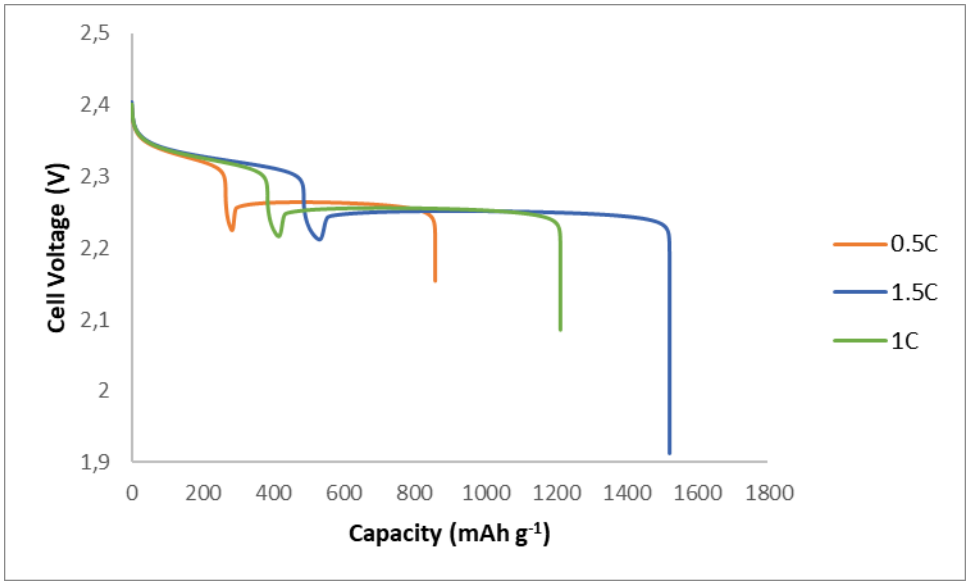

Figure 4.10. Discharge profiles at different discharge rates.

In general, the cell voltage and the discharge capacity are expected to decrease with increasing C-rate [4]. The charge transfer overpotentials increase by increasing the discharge current, reducing the cell voltage. More active material will be lost due to precipitation and the shuttle mechanisms at higher currents. The reaction rates will increase with the increasing current, but the solubility will remain the same. Therefore, the electrolyte will be saturated earlier, and precipitation reactions will cause less S utilization. However, the model prediction shows an opposite trend in Figure 4.10; the discharge capacity increases with higher discharge rates. Since the model is zero-dimensional, the cell's diffusion kinetics and ionic migration are neglected. Hence, the model does not include transport limitations, which increase with the discharge rates.

4.2. One-Dimensional Concentration-Dependent Electrochemical Model

4.2.1. Predictions of the S loading effect on discharge performance

As previously discussed, S loading in the cathode can be controlled in two ways: (i) by changing the C/S ratio in the cathode at a given cathode thickness and (ii) by changing the cathode thickness at a constant C/S ratio. Here, the model predictions are discussed for both cases.

4.2.1.1. C/S Ratio. The C/S ratio is varied to understand its effect on cell behavior. The voltage curves for different C/S ratios are shared below. Carbon amount is crucial for the cathode's active area and conductivity. At the same time, sulfur content should be maximized since sulfur is the active material for the reactions. Consequently, carbon and sulfur contents should be optimized.

The C/S ratio is changed from 0.3 to 8, and the voltage curves are shared herein. For this study, the E/S ratio and the cathode thickness remain constant, and the cell design parameters in Table 3.1 are used. Subsequently, S loading in the cathode changed from 0.86 to 1.06 mg cm^{-2}.

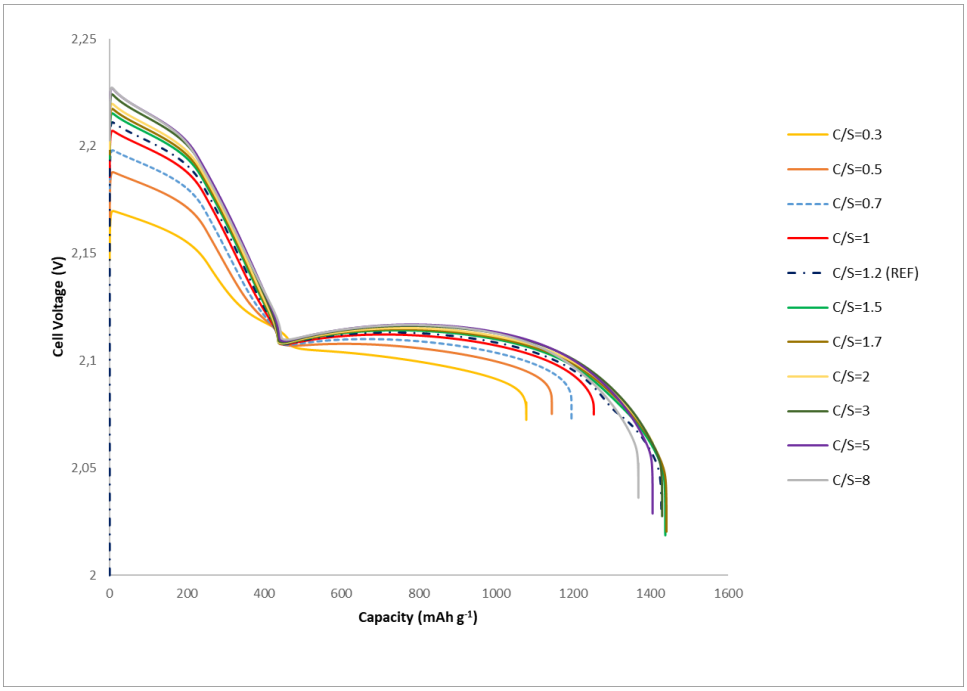

Figure 4.11. Discharge profiles for different C/S ratios at 1C.

As seen in Figure 4.11, the C/S ratio and the capacity are not linearly related. The capacity of the cell increases and then decreases with an increasing C/S ratio. The minimum capacity is observed when the C/S ratio is 0.3, and the maximum value is when the ratio is 1.7. From the results, we can understand that carbon content in the cathode is required to be at a certain level for optimum cell performance. There is a dramatic capacity change when we compare the lower C/S values with each other. On the other hand, adding more carbon

to the cathode does not increase the capacity after a threshold. This may be explained as such. Limited carbon amounts result in poor conductivity and active area for the electrochemical reactions, hurting the kinetics and, thus, the discharge performance. On the other side, by adding too much carbon, the sulfur content will be low, and the active material for the cell will be limited. This predicted trend is typically valid experimentally. For instance, in the study of Michaelis et al. [19], the cathode surface becomes passivated, and the cell is polarized when the sulfur amount is high. Another experimental study investigating the influence of S loading shows that the discharge capacity is reduced at higher S loadings. Since sulfur and low-order polysulfides are insulators, the carbon amount may not be enough to enhance the conductivity in the cathode.

The model can capture the C/S ratio effect successfully because of the cathode active area definition, including the carbon weight fraction and reference porosity terms in Equation (3.40). The model estimates a higher functional area in the cathode with a higher carbon amount, and electrochemical reaction kinetics are enhanced. On the other hand, the increase in the active area and, thus, the capacity stops when the carbon amount increases too much, as it levels off with the decreasing initial porosity. This is an essential modification to the previous models based on Kumarasan et al. since, in those models, the increase in the cell capacity with increasing C/S ratio cannot be captured as the active area is defined independently of the carbon content. Erisen and Eroglu are able to predict the enhancement in the capacity with increasing C/S ratio since they defined the area as a function of the carbon volume fraction; however, this increase is continuous due to the lack of the reference porosity in the definition (if the initial porosity is used instead of a reference porosity in Equation (3.40) the impact of the initial porosity is canceled). So, the one-dimensional model presented here is flexible in defining cell design parameters.

4.2.1.2. Cathode Thickness. Next, the E/S and C/S ratios are kept constant, and to change the sulfur content in the cathode design, the cell thickness is varied. The electrolyte volume fraction and carbon and sulfur weight fractions are kept constant to do that. The model predicts discharge curves with different sulfur loading amounts using the parameters mentioned in Table 3.1, and the curves are shared in Figure 4.12.

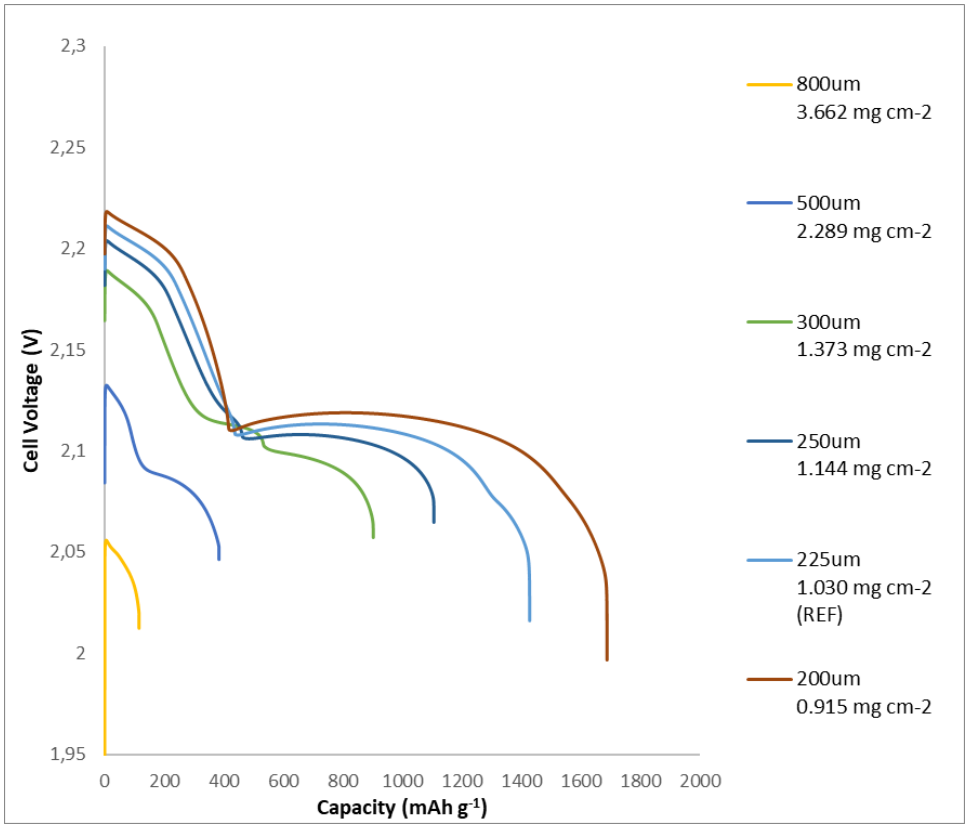

Figure 4.12. Discharge profiles for different cathode thicknesses at 1C.

It is observed in the figure above that the capacity decreases with increasing sulfur loading (or the cathode thickness, in other words). The predicted discharge capacity is at maximum with the thinnest cathode and at minimum with the thickest cathode. Also, the voltage plateaus cannot be recognized for the thicker cathodes. The reaction kinetics get worse by increasing the S loading.

In the literature, several studies observe the same trend experimentally. A study by Kang et al. [20] shows the discharge capacity of [22] Li-S cells with different cathode design parameters. The experimental results are consistent with the model predictions about the effect on the discharge capacity. Increasing S loading leads to disruptions in mass transport. So, even though the active material amount is high, the utilization of the active material will be lower in thicker electrodes. Another study by Sun, Liu, and Gun [21] varies the S loading in the Li-S coin cells. The paper suggests that converting S_4^{2-} to Li_2S_2/Li_2S can be difficult in high S loadings and cause this capacity reduction. Since high currents are applied with increasing sulfur, it is suggested that there is not enough time to form nucleation particles

for Li_2S_2/Li_2S to enhance the reduction reactions. The model is able to predict this trend successfully as such. It defines the cathode porosity depending on the precipitated materials in Equation (3.38). The E/S and C/S ratios are the same for each case; however, the porosity and, thus, the active area in the cathode will change differently during discharge. Higher S loadings can enhance the precipitation reactions, and the model considers the higher loss of cathode porosity and active area. In addition, the C-rate is the same for each case. Therefore, the applied current increases with the S loading. Higher currents lead to a capacity decrease because of earlier saturation in the electrolyte due to high reaction rates.

To sum up, the model can capture the S loading effect (both due to a change in the C/S ratio or the cathode thickness) on the discharge performance of Li-S cells by the active area definition. A one-dimensional model is needed in order to adjust the critical cell design parameters and predict their impact on the performance. A detailed analysis is presented next to study the model's sensitivity to its parameters.

4.2.2. Sensitivity Results

4.2.2.1. Standard Potentials of High and Low Voltage Plateaus. In the model, the standard potentials are used to estimate the OCP for each electrochemical reaction, and then the estimated OCP is involved in the overpotential calculation for each electrochemical reaction that can lead to an effect on the current densities.

Firstly, the standard potential for high voltage plateau is studied. It is increased to 2.35 V and decreased to 2.25 V from 2.30 V, and the voltage curves are compared.

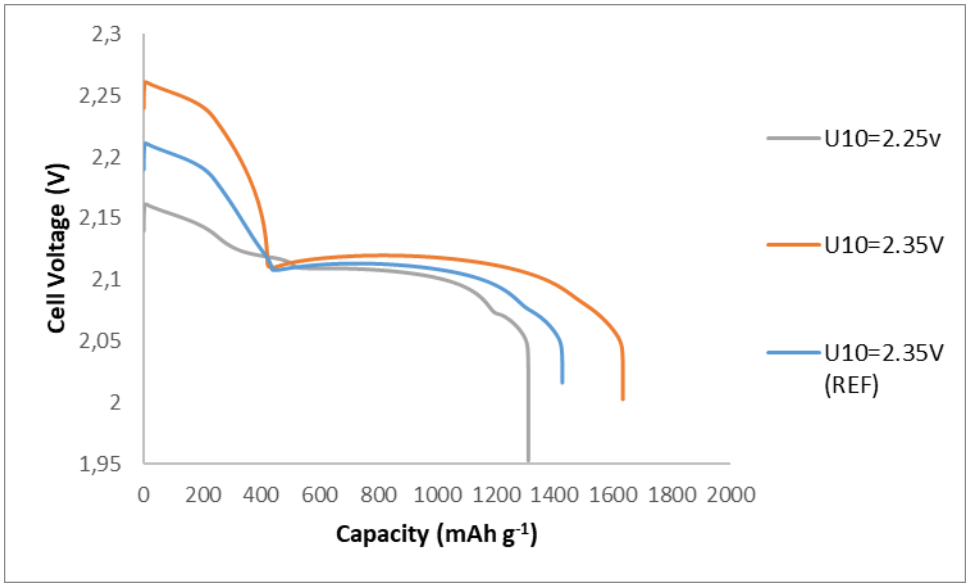

Figure 4.13. Discharge profiles for different standard potentials of high voltage plateau at 1C.

When we compare the voltage curves shown in Figure 4.13, we can say both voltage plateaus are affected by those changes. However, the effect on the first plateau is more straightforward to recognize than on the second plateau. Since the overpotential is affected, the first reaction can be driven forward and accumulate S_4^{2-}. That can provide more reactants for the second reaction and increase capacity. When the lower standard potential decreases the first reaction rate, the active material utilization may be limited for the second region.

The standard potential for low voltage plateau is also changed to 1.97 V, 2.00 V, and 2.03 V.

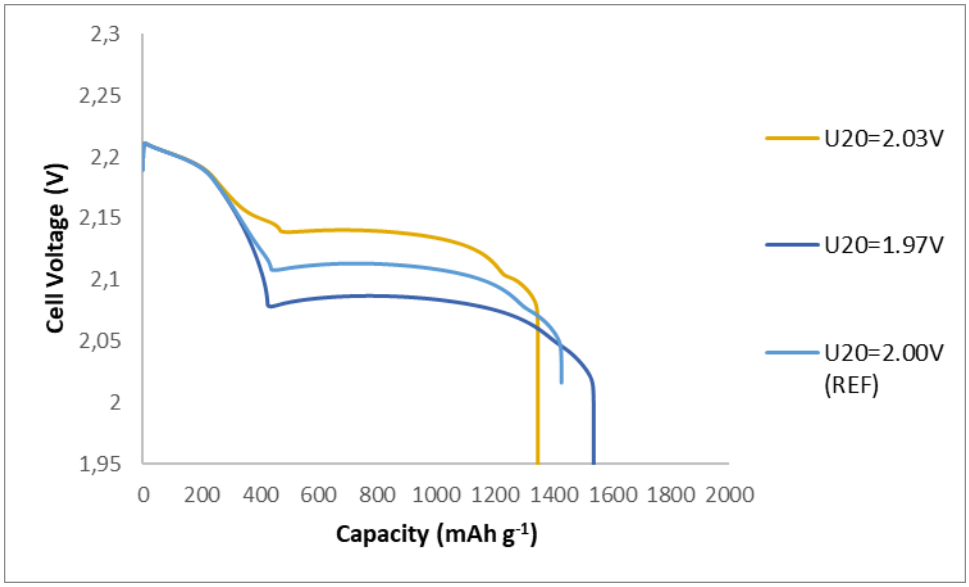

Figure 4.14. Discharge profiles for different standard potentials of low voltage plateau at 1C.

This time, we can see the dominant effect on the second voltage plateau in Figure 4.14. As expected, the reaction rates are affected by the variation of the standard potential. The low voltage plateau is elevated when the reaction rate is higher due to a higher standard potential. On the other hand, increasing the standard potential for low voltage plateau leads to a capacity reduction, as seen in the figure. This may be explained as follows. The consumption of S_4^{2-} increases for a higher standard potential, leading to an accumulation of S^{2-} in the electrolyte. Consequently, more $Li_2S_{(s)}$ will be precipitated, decreasing the cathode porosity and cell capacity. When the standard potential is lower, the production rate of S^{2-} will be less. Therefore S^{2-} will be saturated later, and precipitated $Li_2S_{(s)}$ will be less. Hence, the cathode porosity and the cell capacity will be higher than in the other cases.

4.2.2.2. Exchange Current Density for the First and Second Reactions. The sensitivity analysis also studies the exchange current densities for each electrochemical reaction. As we change the exchange current densities, the reaction rates are affected. The voltage curves are presented in Figure 4.15. The exchange current density for the first reaction is multiplied by a factor of 0.5 and 2.

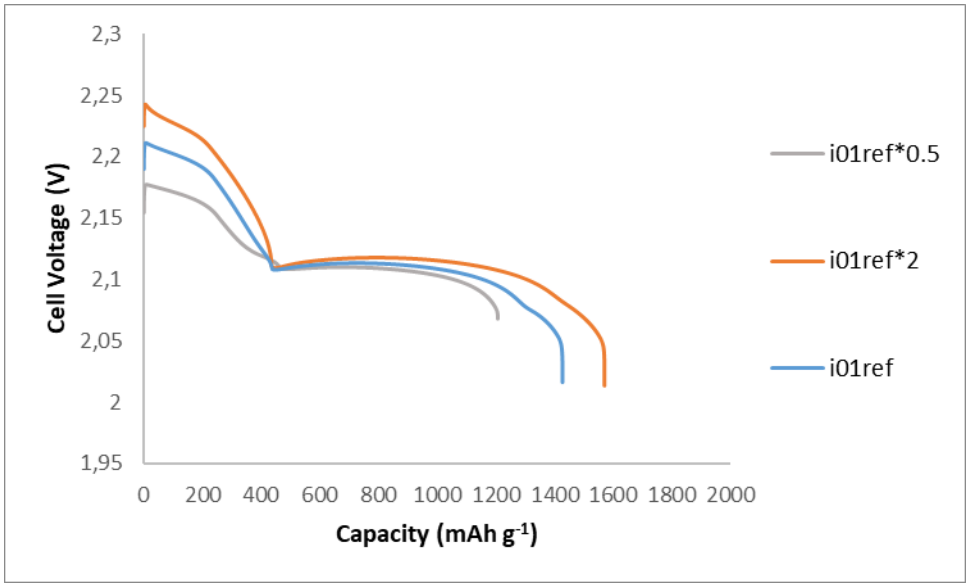

Figure 4.15. Discharge profiles for different first exchange current densities at 1C.

The figure shows that the voltage curve shifts when the exchange current density increases. This shift can be explained by the higher current generated per electrochemical reaction. In addition, the dissolution of S_8^0 can increase since the first reaction will consume S_8^0 at a higher rate. So there will be a positive effect on capacity because of higher utilization of the material. Hence, we can use the same explanation for the opposite case. The consumption rate of S_8^0 will be lower, and that can reduce the dissolution rate of S_8^0. The lower utilization of the material in the first plateau has a negative effect on the total discharge capacity.

For the second reaction exchange current density, three times higher and ten times lower values are compared. The estimated voltage curves are shared in Figure 4.16.

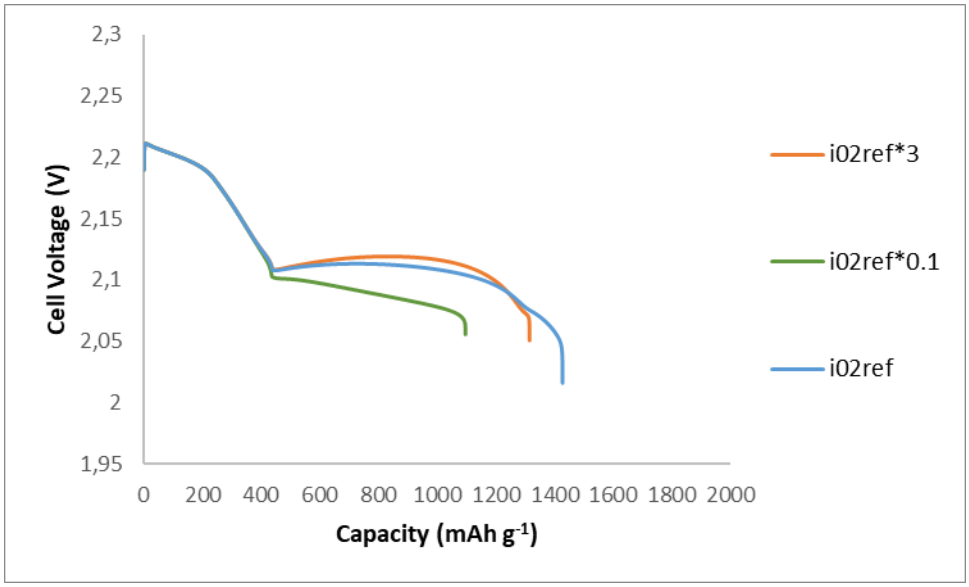

Figure 4.16. Discharge profiles for different second exchange current densities at 1C.

Unlike in Figure 4.15, the effect is limited to the second voltage plateau. The second electrochemical reaction will be slower when the exchange current density is lower, and the precipitation reaction will be dominant. Hence, the capacity will be reduced. When it is higher, the voltage output is higher, as expected, but the consumption rate from the electrochemical reaction will be higher and consume the intermediate product faster. So it will also lead to a capacity reduction.

The study from Ghaznavi and Chen [12] can give some insight into those parameter variations. Since the studied model includes different electrochemical reactions, a direct comparison cannot be made. Nevertheless, the simplified model presented here captures the change in the cell performance and capacity by the exchange current density variation as in the study of Ghaznavi and Chen.

4.2.2.3. Active Surface Area. The active surface area is an essential parameter, according to Abdulkadiroglu, Bektas, and Eroglu [8], and it is included in this sensitivity analysis. The model defines that the electrochemical reactions occur on the available active area, changing during discharge.

The active surface area is multiplied by a factor of two and 0.7 for this analysis.

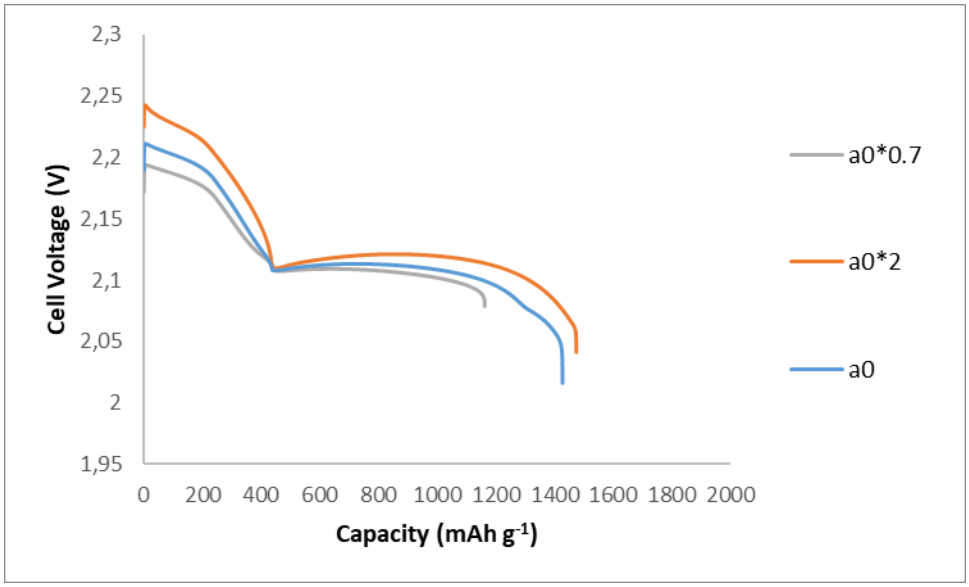

Figure 4.17. Discharge profiles for different active surface areas densities at 1C.

The voltage curves in Figure 4.17 show that the active area predominantly affects both discharge plateaus. When the surface area is high, we expect the electrochemical reaction rates to be higher. Hence, the overpotential will be lower for each reaction. We can see this trend from the obtained voltage curve. In addition, there is an influence on cell capacity. A phenomenological explanation of the capacity change can be the relationship between the electrochemical and precipitation reaction rates. Either one will consume the species more than the other, making its effect more dominant.

4.2.2.4. Precipitation/Dissolution Rates. The precipitation rates for precipitate products, i.e., $Li_2S_{(s)}$ and $S_{8(s)}$, influence the consumption rate of species. They are included in the definition of *R'* in the governing equations.

For this study, the precipitation rate constant of $Li_2S_{(s)}$ is multiplied by a factor of five and 0.2. The voltage curves are shown in Figure 4.18.

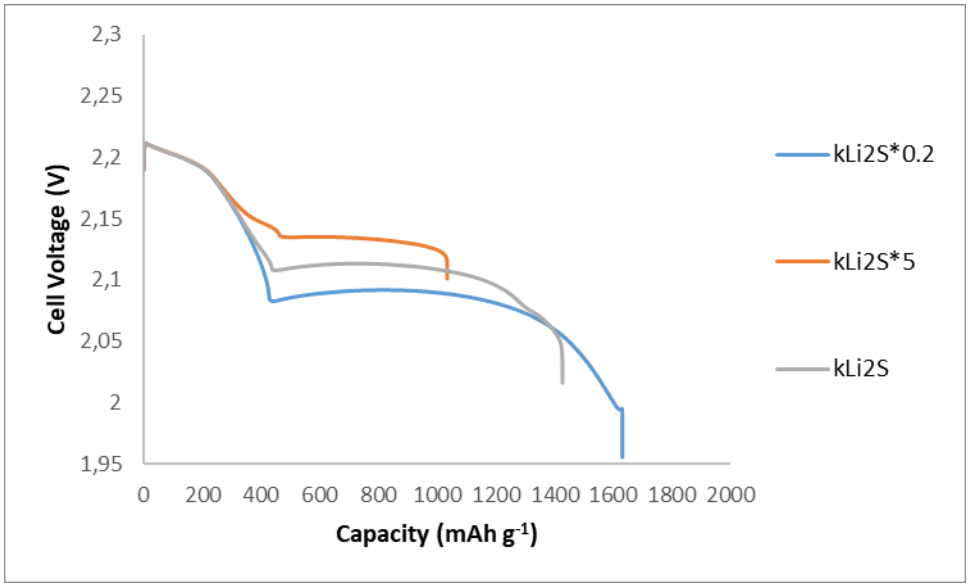

Figure 4.18. Discharge profiles for different $Li_2S_{(s)}$ precipitation constants at 1C.

When $Li_2S_{(s)}$ precipitation rate is high, Li^+ and S^{2-} ions can be consumed more. Due to the low concentration of S^{2-}, the second reaction will be driven forward. Moreover, the volume fraction of $Li_2S_{(s)}$ precipitate will increase and affect cell performance negatively because it lowers the porosity of the cathode. The opposite effect can be observed from the voltage curve. More S^{2-} ions will be available in the electrolyte, and thus the second plateau capacity increases. With a reduced precipitation rate, cathode porosity will increase, leading to an increase in the capacity, as experimentally studied by Kang et al. [20].

The precipitation rate constant of $S_{8(s)}$ is increased by a factor of three and 0.8, and the voltage curves taken from the model are presented in Figure 4.19.

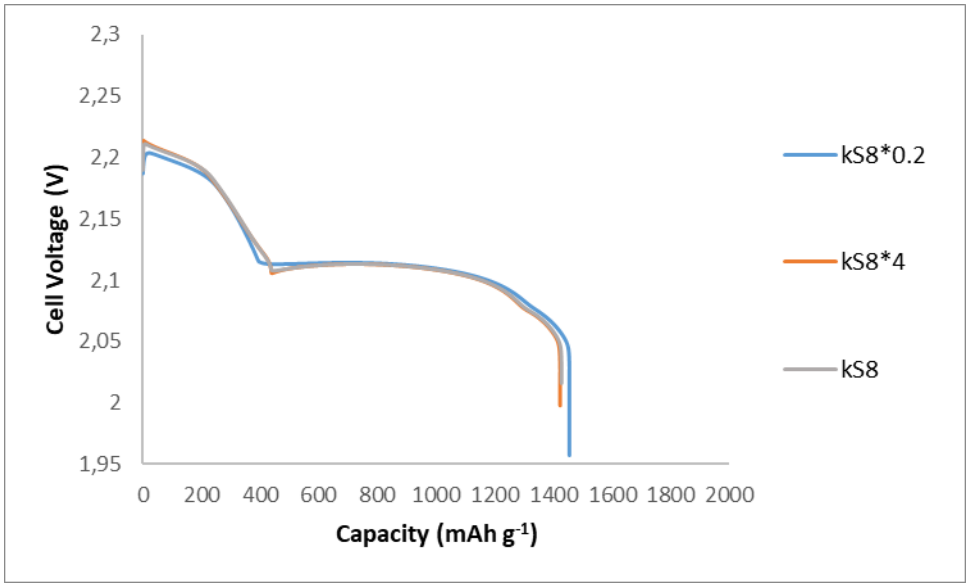

Figure 4.19. Discharge profiles for different $S_{8_{(s)}}$ precipitation constants at 1C.

When the precipitation rate is lower, a slight shift in the voltage curve can be seen. $S_{8_{(s)}}$ dissolution rate will be lower at the start. A lower concentration of S_8^0 can have a negative effect on the first plateau. On the other hand, the voltage curve overlaps with the reference curve when the rate is higher. If dissolved S_8^0 does not exceed the solubility threshold, we will not see any effect. Nevertheless, we can conclude that the dissolution/precipitation rate variation has a minimal effect on the cell capacity.

4.2.2.5. Solubility. The solubility of the precipitates is analyzed for both $Li_2S_{(s)}$ and $S_{8(s)}$. The relationship between dissolution and precipitation depends on the solubility threshold.

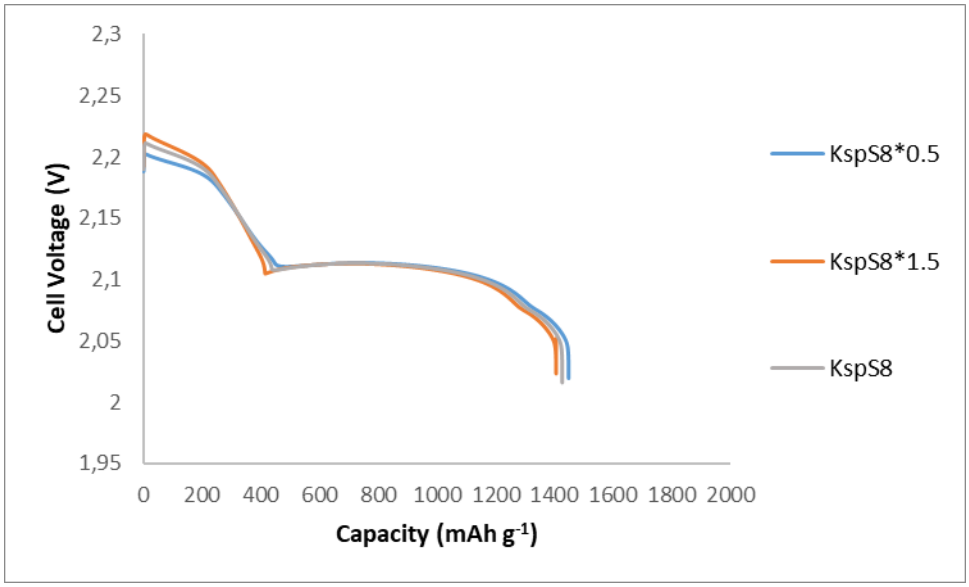

Figure 4.20. Discharge profiles for different $S_{8_{(s)}}$ solubility constants at 1C.

For $S_{8(s)}$ solubility, the rate constant is changed to 1.5 and 0.5 times the reference value. The voltage shift is slightly recognizable for both cases in Figure 4.20. When solubility increases, the concentration of S_8^0 will be higher in the cathode. So, the rate of the electrochemical reactions increase. In addition, the higher amount of S_8^0 can drive forward the precipitation reaction of $Li_2S_{(s)}$. So that can be the reason for the slight capacity decrease. We can expect the opposite when it is lower since the S_8^0 will be saturated and precipitate earlier.

For studying the effect of $Li_2S_{(s)}$ solubility, the rate constant is multiplied by a factor of 100 and 0.01. The voltage curves are shared in Figure 4.21.

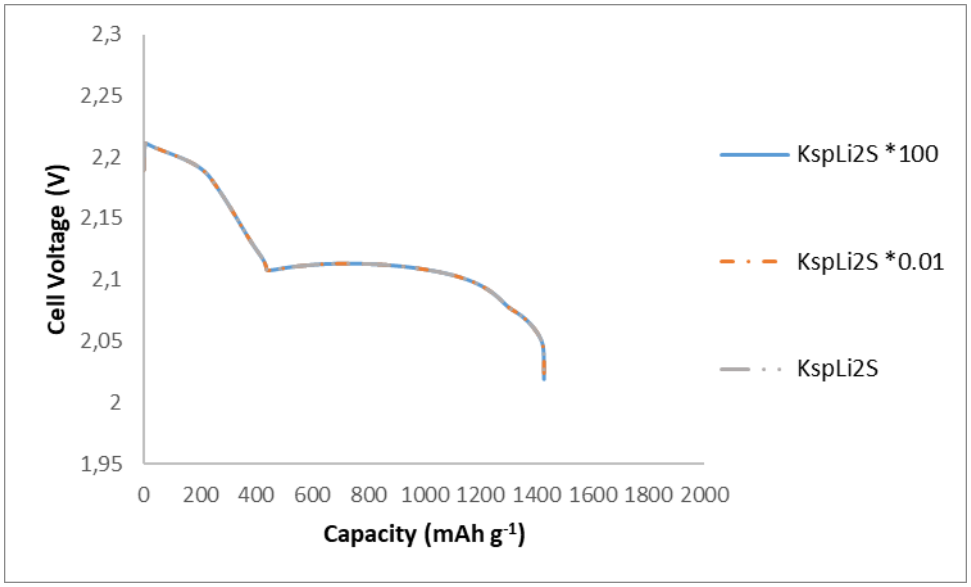

Figure 4.21. Discharge profiles for different $Li_2S_{(s)}$ precipitation constants at 1C.

Li^+ ion content will be higher in the cathode when solubility is increased. However, the voltage curves do not show any variance for different K_{sp} values. There can be another limiting step; for example, the dissolution rate cannot be high enough to reach the solubility level, or the model is not sensitive to this parameter.

4.2.2.6. C-rate. The simulated cell voltage curves at 1.5C and 1C are shared in Figure 4.22.

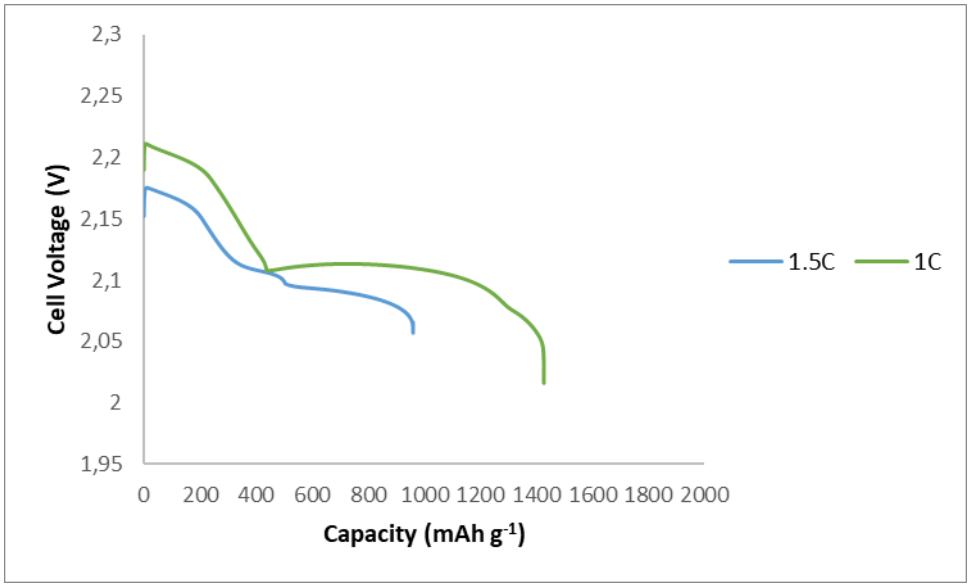

Figure 4.22. Discharge profiles at different discharge rates.

The figure shows capacity reduction with the increasing discharge rate, which matches the experimental results [4]. The S utilization becomes less because of the saturated electrolyte and precipitation reactions at high discharge rates.

On the other hand, the computational time becomes very long as lower discharges than 1C are applied. Therefore, the model could be improved for low discharge rates.

5. CONCLUSION

The thesis investigated the effect of the critical parameter S loading on the discharge performance of Li-S cells using two different mathematical models. One model was zero-dimensional, and the other one was one-dimensional. The predictions from the models were compared, and sensitivity analysis was done for each. Firstly, the results from the zero-dimensional model were shared and discussed. The zero-dimensional model did not define any cathode design parameters; however, active sulfur mass in the cell was changed to estimate the effect of S loading. The predictions from the model showed us that there is no discharge capacity change when the sulfur mass is varied. The zero-dimensional model predictions were inconsistent with the experimental data. For sensitivity analysis, various parameters were changed. The model predictions showed a change in the active area, but it was limited to the voltage output. When the initial voltage was changed, there was a slight change at the beginning of the high voltage plateau and a slight capacity decrease at the lower initial voltage. The standard potentials showed a significant effect on the discharge performance. When the gap between the potentials was increased, the predicted performances were enhanced. The change in the exchange current densities showed only voltage shifts in the related voltage plateau. Also, varying the precipitation rate constant did not change the estimations of discharge capacity. We saw a capacity change when the shuttle constant and the c-rate were varied. However, the c-rate effect is different from the experimental studies in the literature. This inconsistency can be caused by neglecting transport kinetics due to the nature of the zero-dimensional model. On the other hand, the one-dimensional model captured the experimental trend on S loadings. The model's cathode active area modification by Abdulkadiroglu, Bektas, and Eroglu [21] helped accurately estimate the effect of S loading. Also, the one-dimensional model was flexible enough to vary the C/S ratio and the cathode thickness separately. Then, the results of the sensitivity analysis were shared and discussed. The model showed high sensitivity to all model parameters except for $K_{sp_{Li_2S(s)}}$.

Overall, the zero-dimensional model is simpler and faster for predicting the discharge performance of Li-S batteries. The requirement of using the zero-dimensional model is to simplify the process and eliminate the assumed parameters, but the investigated model could

not predict the effect of the cathode design parameters, especially the S-loading. On the contrary, the one-dimensional model shows successful predictions. The main difference between the models is that the one-dimensional model includes the transport kinetics and cathode material definitions. These kinetics and definitions can be crucial to capture the practical effects of cathode design. In order to capture the effects of S-loading, the investigated zero-dimensional model cannot be a simple alternative to the one-dimensional model.

For future work, different models can be investigated. For example, the study of Zhang et al. [16], another zero-dimensional model, defines the porosity in the model. The definition can be modified if necessary to estimate the effect of cathode design parameters on the discharge performance. On the other hand, the one-dimensional model is not very useful due to computational time when the discharge rate is low; this can be an improvement point.

REFERENCES

1. Kumaresan K., Y. Mikhaylik, and R. E. White, “A Mathematical Model for a Lithium–Sulfur Cell”, *Journal of the Electrochemical Society*, Vol. 155, No. 8, p. A576, 2008.

2. Zhao X., G. Cheruvally, C. Kim, K.-K. Cho, H.-J. Ahn, K.-W. Kim, and J.-H. Ahn, “Lithium/Sulfur Secondary Batteries: a Review”, *Journal of Electrochemical Science and Technology*, Vol. 7, No. 2, pp. 97–114, 2016.

3. Shao Q., S. Zhu, and J. Chen, “A Review on Lithium-Sulfur Batteries: Challenge, Development, and Perspective”, *Nano Research*, Vol. N/A, No. N/A, pp. N/A, 2023.

4. Bilal H. M. and D. Eroglu, “Carbon-to-Sulfur Ratio in the Cell Controls the Discharge Capacity, Cycling Performance and Energy Density of a Lithium-Sulfur Battery,” *International Journal of Energy Research*, Vol. 46, No. 11, pp. 15926–15937, 2022.

5. Erisen N., N. B. Emerce, S. C. Erensoy, and D. Eroglu, “Modeling the Effect of Key Cathode Design Parameters on the Electrochemical Performance of a Lithium-Sulfur Battery”, *International Journal of Energy Research*, Vol. 42, No. 8, pp. 2631–2642, 2018.

6. Eroglu D., K. R. Zavadil, and K. G. Gallagher, “Critical Link between Materials Chemistry and Cell-Level Design for High Energy Density and Low Cost Lithium-Sulfur Transportation Battery”, *Journal of the Electrochemical Society*, Vol. 162, No. 6, pp. A982–A990, 2015.

7. Marinescu M., T. Zhang, and G. J. Offer, “A Zero Dimensional Model of Lithium-Sulfur Batteries During Charge and Discharge”, *Physical Chemistry Chemical Physics*, Vol. 18, No. 1, pp. 584–593, 2016.

8. Abdulkadiroglu B., H. Bektas, and D. Eroglu, “How to Model the Cathode Area in Lithium-Sulfur Batteries?”, *Chemelectrochem*, Vol. 9, No. 4, pp. e202101553, 2022.

9. Erisen N. and D. Eroglu, “Modeling the Discharge Behavior of a Lithium-Sulfur Battery”, *International Journal of Energy Research*, Vol. 44, No. 13, pp. 10599–10611, 2020.

10. Ghaznavi M. and P. Chen, “Sensitivity Analysis of a Mathematical Model of Lithium-Sulfur Cells Part I: Applied Discharge Current and Cathode Conductivity”, *Journal of Power Sources*, Vol. 257, pp. 394–401, 2014.

11. Ghaznavi M. and P. Chen, “Sensitivity Analysis of a Mathematical Model of Lithium-Sulfur Cells: Part II: Precipitation Reaction Kinetics and Sulfur Content”, *Journal of Power Sources*, Vol. 257, pp. 402–411, 2014.

12. Ghaznavi M. and P. Chen, “Analysis of a Mathematical Model of Lithium-Sulfur Cells Part III: Electrochemical Reaction Kinetics, Transport Properties and Charging”, *Electrochimica Acta*, Vol. 137, pp. 575–585, 2014.

13. Mikhaylik Y. V. and J. R. Akridge, “Polysulfide Shuttle Study in the Li/S Battery System”, *Journal of the Electrochemical Society*, Vol. 151, No. 11, p. A1969, 2004.

,

14. Yoo K., M. K. Song, E. J. Cairns, and P. Dutta, “Numerical and Experimental Investigation of Performance Characteristics of Lithium/Sulfur Cells”, *Electrochimica Acta*, Vol. 213, pp. 174–185, 2016.

15. Marinescu M., L. O’Neill, T. Zhang, S. Walus, T. E. Wilson, and G. J. Offer, “Irreversible vs Reversible Capacity Fade of Lithium-Sulfur Batteries during Cycling: the Effects of Precipitation and Shuttle”, *Journal of the Electrochemical Society*, Vol. 165, No. 1, pp. A6107–A6118, 2018.

16. Zhang T., M. Marinescu, L. O’Neill, M. Wild, and G. Offer, “Modeling the Voltage Loss Mechanisms in Lithium-Sulfur Cells: The Importance of Electrolyte Resistance

and Precipitation Kinetics", *Physical Chemistry Chemical Physics,* Vol. 17, No. 35, pp. 22581–22586, 2015.

17. Zhang T., M. Marinescu, S. Walus, P. Kovacik, and G. J. Offer, "What Limits the Rate Capability of Li-S Batteries during Discharge: Charge Transfer or Mass Transfer?", *Journal of the Electrochemical Society,* Vol. 165, No. 1, pp. A6001–A6004, 2018.

18. Andrei P., C. Shen, and J. P. Zheng, "Theoretical and Experimental Analysis of Precipitation and Solubility Effects in Lithium-Sulfur Batteries", *Electrochimica Acta,* Vol. 284, pp. 469–484, 2018.

19. Michaelis C., N. Erisen, D. Eroglu, and G. M. Koenig, "Electrochemical Performance and Modeling of Lithium-Sulfur Batteries with Varying Carbon to Sulfur Ratios", *International Journal of Energy Research,* Vol. 43, No. 2, pp. 874–883, 2019.

20. Kang N., Y. Lin, L. Yang, D. Lu, J. Xiao, Y. Qi, and M. Cai, "Cathode Porosity Is a Missing Key Parameter to Optimize Lithium-Sulfur Battery Energy Density", *Nature Communications*, Vol. 10, No. 1, pp. 1–10, 2019.

21. Sun K., H. Liu, and H. Gan, "Cathode Loading Effect on Sulfur Utilization in Lithium-Sulfur Battery", *Journal of Electrochemical Energy Conversion and Storage,* Vol. 13, No. 2, pp. 1–9, 2016.

22. Ding N., S. W. Chien, T. S. A. Hor, Z. Liu, and Y. Zong, "Key Parameters in Design of Lithium Sulfur Batteries", *Journal of Power Sources*, Vol. 269, pp. 111–116, 2014.

23. Newman J. S. and K. E. Thomas-Alyea, *Electrochemical Systems*, John Wiley & Sons, New Jersey, 2004.

24. Gao J. and H. D. Abruña, "Key Parameters Governing the Energy Density of Rechargeable Li/S Batteries", *Journal of Physical Chemistry Letters*, Vol. 5, No. 5, pp. 882–885, 2014.

25. Emerce N. B. and D. Eroglu, “Effect of Electrolyte-to-Sulfur Ratio in the Cell on the Li-S Battery Performance”, *Journal of the Electrochemical Society*, Vol. 166, No. 8, pp. A1490–A1500, 2019.